Journal of Molecular Modeling (2021) 27: 286
https://doi.org/10.1007/s00894-021-04886-y

ORIGINAL PAPER

Investigation of structural evolution in the Cu–Zr metallic glass at cryogenic temperatures by using molecular dynamics simulations

Akash A. Deshmukh[1] · Jatin G. Bhatt[2] · Prashant M. Gade[3] · Snehanshu Pal[1]

Received: 27 December 2020 / Accepted: 19 August 2021 / Published online: 15 September 2021

Abstract

In the present work, investigation of structural evolution of $Cu_{33}Zr_{67}$ specimen during the cooling process from 2500 down to the 300 K, 200 K, 150 K, 100 K, 50 K, and 10 K has been performed at cooling rate of 5 K/ps using molecular dynamics simulation. The pair distribution function (PDF) reveals that Zr−Zr pair causes the splitting of the first peak of the $Cu_{33}Zr_{67}$ glass at a lower temperature with an increase in height. Splitting of the first and second peaks supports the presence of the inhomogeneous structure with a statistical average of crystal-like and disordered structural regions in the $Cu_{33}Zr_{67}$ glass. Voronoi cluster analysis indicated that quasi icosahedral clusters such as <284>, <0285>, and <0282>; mixed-type cluster such as <0364>; and crystal-like clusters such as <0446> are responsible for stabilization of glassy phase at 300 K, 200 K, 150 K, 100 K, 50 K, and 10 K. Similarly, the maximum population of the Cu-centered and Zr-centered <0286> quasi icosahedral clusters support the stability of the glassy phase over the studied temperature range. Besides, the maximum population of Cu-centered <0367> and Zr-centered <0364>, <0367>, <0363>, and <0365> mixed-type clusters and Cu-centered <0448> and Zr-centered <0448>, <0445>, <0446>, and <0444> crystal-like clusters support the possibility of the presence of intermediate phase of $CuZr_2$ at lower temperatures as observed from PDFs. Mean square displacement (MSD) for the $Cu_{33}Zr_{67}$ glass shows that the diffusion coefficient of Cu and Zr atoms reduces with decreasing temperature from 300 to 10 K. Diversity parameter (d) was found to decrease with decreasing temperature.

Keywords Molecular dynamics (MD) simulations · Cryogenic temperatures · Voronoi clusters · Mean square displacement (MSD) · Diversity (d)

Introduction

It is known that the excellent mechanical properties of metallic glasses (MGs) such as high elasticity and strength, high corrosion resistance, and hardness are overshadowed by their intrinsic brittleness [1, 2]. Therefore, improving the ductility, plasticity, and hardness of the MGs has been subject of immense interest [1, 2]. In recent years, different nanostructures have been widely used as reinforcement materials to improve the mechanical properties for polymers [3, 4] and metallic glasses [1, 5–7]. Earlier studies to improve the mechanical properties of $Cu_{25}Zr_{75}$, $Cu_{50}Zr_{50}$, and $Cu_{75}Zr_{25}$ MGs have shown that the reinforcement by nanofillers is independent of the chemical compositions of the alloys [1, 6, 7]. On the other hand, attempts were also made to improve the strength and increase the fracture toughness of the alloys for cryogenic structural applications [8]. Although the high strength of the material can be achieved by reducing thermal activation at cryogenic temperatures, it is difficult to achieve improved toughness in ordinary alloys [8–10]. Besides, earlier reports [11–14] have shown the possibility to achieve high strength with improved ductility in bulk metallic glasses (BMGs) at low temperatures. High yield strength along with high fracture toughness at cryogenic temperatures in BMGs is achievable by reducing shear–band viscosity, shear–slip velocity, and the stress drop in the serrated flow [12, 13]. Therefore, the knowledge

✉ Akash A. Deshmukh
akdeshmukh9@gmail.com

[1] Department of Metallurgical and Materials Engineering, National Institute of Technology, Rourkela 769008, Odisha, India

[2] Department of Metallurgical and Materials Engineering, VNIT, Nagpur 440010, MS, India

[3] Computaional Physics Laboratory, Department of Physics, Rashtasant Tukadoji Maharaj Nagpur University, Nagpur 440033, MS, India

of the effect of thermal activation of metallic glasses (MGs) on the change of physical properties is necessary for predicting the material behavior for their practical applications [15]. Recent studies have suggested that the medium-range order (MRO) clusters are connected via a fractal network with a dimension of 2.31 in BMGs [16, 17]. These clusters are responsible for the stable glassy phase thereby providing resistance to the nucleation and growth of crystalline phases [18, 19]. In particular, it has shown that the presence of full icosahedra < 00,120 > is one of the most important Voronoi clusters (VCs) for the stability of the MGs [20, 21]. The VC < 00120 > is responsible for the slowing down of relaxation dynamics compared to other polyhedral [20, 21]. Recently, Cu–Zr binary glasses [22–25] have been investigated for their mechanical properties such as tensile strength, surface damage under the impact of a nanosized projectile. Additionally, CuZr-based BMGs [26–28] were also studied due to their enhanced mechanical properties at room temperature. However, the fundamental understanding of the glass-forming mechanism and its effect on properties is still unclear at cryogenics. This alloy provides a large compositional range from 25 to 72 at % of Cu to explore the structural dynamics at the atomic level and its relationship with glass-forming ability (GFA) [29, 30].

Earlier, Kluge, and Schober [31, 32] have studied the diffusion and jump length in the $Cu_{33}Zr_{67}$ glass from 2000 to 700 K with different cooling rates. Similarly, Han and Schober [33] and Liu et al. [34] have reported the diffusion studies in the temperature range of 2400 to 1200 K and 2000 to 800 K, respectively, in $Cu_{33.3}Zr_{66.7}$ glass. However, the study of this glassy alloy was not addressed at lower temperatures which have created a lack of understanding in glass behavior under cryogenic conditions. The significance of the low-temperature applications and the importance of the $Cu_{33}Zr_{67}$ glass have motivated us to perform the low-temperature studies of the $Cu_{33}Zr_{67}$ glass from 300 to 10 K and address the structural evolution at the atomic scale using molecular dynamics (MD) simulations. In the present work, MD has been used to address the GFA and the structural evolution with temperature. Our overall goal of the present study is to address the underlying physical mechanism responsible for the structural rearrangements during cooling from 300 to 10 K in $Cu_{33}Zr_{67}$ alloy and its role in GFA. The role of different Voronoi polyhedral clusters behind the glass-forming mechanism at the atomic scale has also been evaluated.

Computational details

An investigation of structure evolution during the cooling process from 300 to 10 K was performed for $Cu_{33}Zr_{67}$ by MD simulations using Large-scale Atomic/Molecular Massively Parallel Simulator (LAMMPS) platform [35]. Embedded atom method (EAM) interatomic potential developed by Mendelev et al. [36] has been used. A simulation box of 10 nm × 10 nm × 10 nm dimensions containing approximately 87,808 atoms has been constructed by applying the periodic boundary condition. The motion equations were solved by the velocity–Verlet algorithm in the velocity form [37]. The isothermal–isobaric ensemble (i.e., NPT) with a constant atom number (N), pressure (P), and temperature (T) have been used. The temperature is controlled by Nose–Hoover thermostat [38], and zero pressure is maintained using Nose–Hoover barostat [39, 40], respectively. The specimen has been heated from 300 to 2500 K with a time step of 0.002 ps at a heating rate of 5 K/ps. Further, the specimen has been equilibrated at 2500 K for 50 ps and then cooled down to 300 K, 200 K, 150 K, 100 K, 50 K, and 10 K at a cooling rate of 5 K/ps. From the literature survey [1, 6, 7, 19–25, 29–34, 37, 40–43], it has been observed that Cu−Zr binary MGs and Cu−Zr-based MGs have been quenched at different temperatures with a wider cooling rate (R_C) ranging from 0.04 to 500 K/ps. Among them, $Cu_{33}Zr_{67}$ was studied at R_C of 0.04 K/ps, 0.2 K/ps, 1 K/ps, and 5 K/ps, 25 K/ps by Kluge et al. [31, 32]. Similarly, Han et al. [33] and Liu et al. [34] investigated the $Cu_{33.3}Zr_{66.6}$ MGs at R_C of 1 K/ps and 0.4 K/ps, respectively. Being large in atomic size (Zr_{radius}, 1.603 Å) [44] compared to that of Cu (Cu_{radius}, 1.278 Å) [44], it was presumed that the introduction of Zr in Cu will re-structure the geometry of the Cu leading to the new geometrical arrangement at atomic scale in binary $Cu_{33}Zr_{67}$ MG. Moreover, Zhang et al.[41] have reported that the orientation of the crystalline structure becomes more prominent at lower cooling rate, i.e., 10 K/ps for 2D Cu. Considering all these aspects, it was proposed that the use of lower cooling rate, i.e., 5 K/ps, would provide significant structural evolution at lower temperatures. On the other hand, $Cu_{46}Zr_{54}$ [45] and Cu−Zr−Ag [46] MGs have been studied at the same heating rate (R_h) and cooling rate (R_C) in addition to the different R_C to study their effect on thermal properties of the system. Like R_C, there is a critical heating rate (R_h) to maintain the amorphous structure while heating to the liquid state [47]. It indicates the lowest heating rate required to avoid devitrification when heating a perfect amorphous sample to a liquid in equilibrium [47]. Earlier [47–49], it was reported that the difference in R_C and R_h causes asymmetry in crystallization and divarication. Therefore, to avoid any such discrepancy and to investigate the structural evolution in $Cu_{33}Zr_{67}$ as function of temperature alone in the present work, both R_h and R_C were kept identical, i.e., 5 K/ps. The structural details have been retrieved by pair distribution function (PDF) [50, 51], coordination number (CN), and Voronoi cluster

(VC) analysis [29, 52, 53]. Mean square displacement (MSD) [54] studies for Cu and Zr atoms have also been performed in the temperature range of 300 to 10 K. MSD will provide information on the atomic diffusion of the different atomic species such as Cu and Zr. Equation (1) is for the calculation of MSD [54].

$$MSD = \left\langle r^2(t) \right\rangle = \left\langle \frac{1}{N} \sum_{i=0}^{N} \left(r_i(t) - r_i(0) \right)^2 \right\rangle \quad (1)$$

In Eq. (1), N represents the number of atoms, t is the time duration, and $r_i(t) - r_i(0)$ is the vector distance traveled by a specific atom over the time duration. Besides, diversity (d) in the clusters at different temperatures is also evaluated.

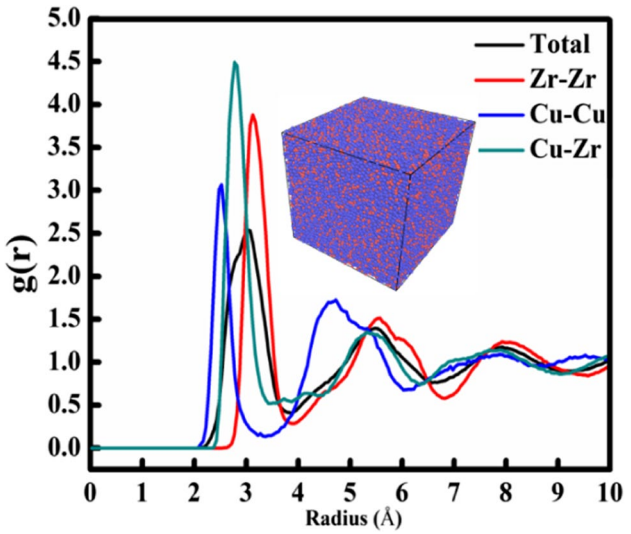

Fig. 1 Total and partial PDFs of $Cu_{33}Zr_{67}$ MGs. The inset is a 3D configuration of $Cu_{33}Zr_{67}$ MG. The red and blue balls represent Cu and Zr atoms, respectively

Results and discussion

Pair distribution functions (PDFs)

For obtaining interatomic distances and coordination number (CNs) of the rapidly quenched specimen of the $Cu_{33}Zr_{67}$ MG, total pair distribution function (PDF) and partial pair distribution function (pPDF) have been studied. Figure 1 shows the typical nature of the total and pPDF at 300 K with the 3D specimen structure of the $Cu_{33}Zr_{67}$ glassy alloy. Variations in total PDFs of the liquid to the glassy state of $Cu_{33}Zr_{67}$ with decreasing temperature have been illustrated in Fig. 2.

Splitting of the first peak with a sharp increase in its height has been observed in Fig. 2, while quenching the liquid melt from 2500 to 10 K. The height of the second sub-peak was found to be increasing monotonically irrespective of the first sub-peak when the temperature decreases from 300 to 10 K. Similarly, the evolution of the splitting of the second peak has also been noticed at 300 K compared to that of 2500 K. The first sub-peak of the second main peak has been found to increase monotonously as the temperature decreases down to 10 K from 300 K irrespective of the second sub-peak. Besides, a small peak between the first and second main peaks is found to grow with decreasing temperature. To elucidate the splitting mechanism of the first and second peaks, pPDFs have been carried out for Cu–Cu, Cu–Zr, and Zr–Zr pairs as shown in Fig. 3 Identical illustration, as observed in Fig. 2, of the increasing magnitude of the first peak and its splitting has been observed in $g_{Zr-Zr}(r)$ as shown in Fig. 3c. Like Fig. 2, splitting of the second peak has been noticed for $g_{Cu-Cu}(r)$ and $g_{Zr-Zr}(r)$ in Fig. 3a and c respectively. Splitting of the second peak of the PDF and pPDF is the indicator of the formation of the glassy state [34]. Growth of the first sub-peak with lowering temperature was found to be more pronounced compared to

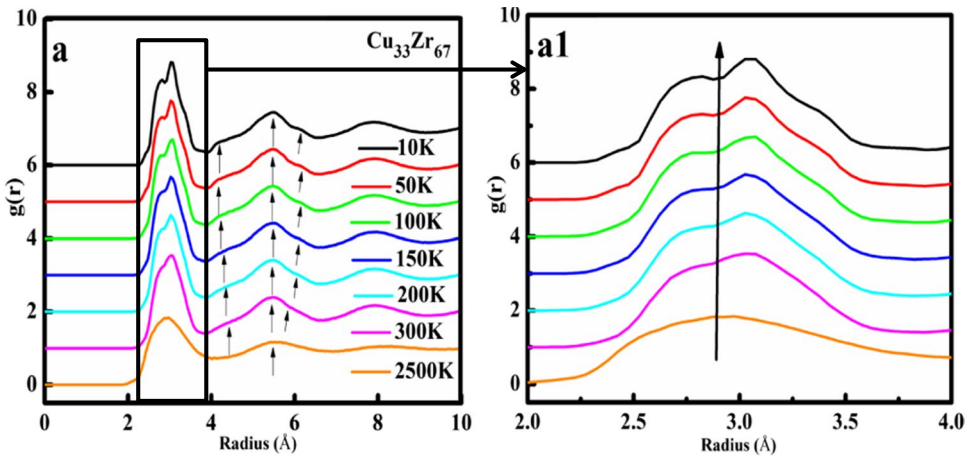

Fig. 2 **a** Total PDFs of $Cu_{33}Zr_{67}$ MG at 300 K, 200 K, 150 K, 100 K, 50 K, 10 K obtained using MD simulations. **a1** g(r) in the range of 2.0 to 4.0 Å.

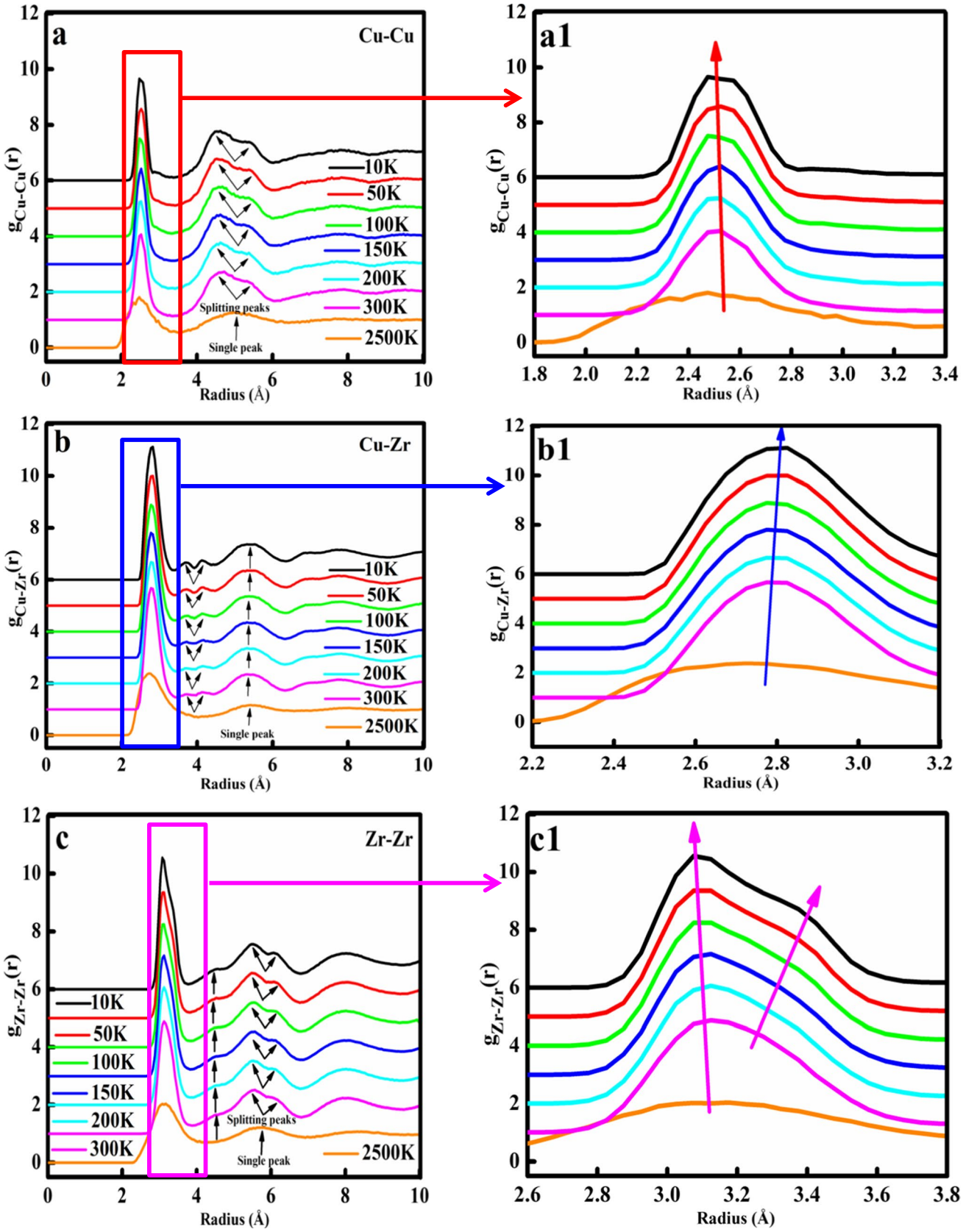
a
Cu-Cu
$g_{Cu-Cu}(r)$
10K
50K
100K
150K
200K
300K
2500K
Splitting peaks
Single peak
Radius (Å)
a1
$g_{Cu-Cu}(r)$
Radius (Å)
b
Cu-Zr
$g_{Cu-Zr}(r)$
10K
50K
100K
150K
200K
300K
2500K
Single peak
Radius (Å)
b1
$g_{Cu-Zr}(r)$
Radius (Å)
c
Zr-Zr
$g_{Zr-Zr}(r)$
10K
50K
100K
150K
200K
300K
2500K
Splitting peaks
Single peak
Radius (Å)
c1
$g_{Zr-Zr}(r)$
Radius (Å)

◂**Fig. 3** Partial PDFs of $Cu_{33}Zr_{67}$ MG for **a** $g_{Cu\text{-}Cu}(r)$, **b** $g_{Cu\text{-}Zr}(r)$, and **c** $g_{Zr\text{-}Zr}(r)$ at 300 K, 200 K, 150 K, 100 K, 50 K, 10 K obtained using MD simulations. **a1**, **b1**, and **c1** represent partial g(r) for $g_{Cu\text{-}Cu}(r)$, $g_{Cu\text{-}Zr}(r)$, and $g_{Zr\text{-}Zr}(r)$ in the range of 1.8 to 3.4 Å, 2.2 to 3.2 Å, and 2.6 to 3.8 Å, respectively

that of the second sub-peak in $g_{Cu–Cu}(r)$ and $g_{Zr–Zr}(r)$. Unlike $g_{Cu–Cu}(r)$ and $g_{Zr–Zr}(r)$, no splitting of the second peak has been observed for $g_{Cu–Zr}$ (r) in Fig. 3b. However, at 300 K onwards, two small unusual peaks were found to emerge at the minimum of the first peak on the higher *R* side of $g_{Cu–Zr}(r)$ as noticed in Fig. 3b. The second sub-peak was found to increase with lowering the temperature compared to that of the first sub-peak. An increase in height of one such peak has also been noticed for $g_{Zr–Zr}(r)$ in Fig. 3c. From these observations, it can be presumed that with lowering the temperature from 300 to 10 K, atoms are trying to arrange themselves in some order fashion leading to the coexistence of the crystal-like and disordered structural region which will be discussed in detail in the section "Proposed crystal structure evolution during cooling from 300 to 10 K." Besides, in Fig. 3a1, b1, and c1, intensity and height of the peaks at different temperatures have been enlarged. These figures show that the peak of the $g_{Cu–Cu}(r)$ shifts towards the lower *R* value with decreasing temperatures. Similarly, the peak of the $g_{Cu–Zr}(r)$ is found to shift towards higher *R* values with decreasing temperature. On the other hand, splitting of the first peak in the opposite directions for $g_{Zr–Zr}(r)$ can be seen in Fig. 3c1. Competition of first peaks in $g_{Cu–Cu}(r)$, $g_{Cu–Zr}(r)$, and $g_{Zr–Zr}(r)$ to grow in opposite directions with decreasing temperature is responsible for splitting of the first peak in total PDF as shown in Fig. 2. To shed a light on such peculiar behavior, in Fig. 4, variations in interatomic distances

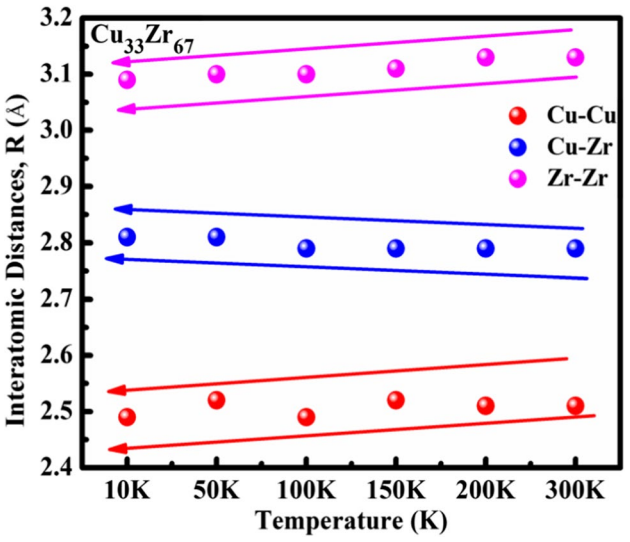

Fig. 4 Variation in interatomic distances obtained by MD simulations at 300 K, 200 K, 150 K, 100 K, 50 K, 10 K for $Cu_{33}Zr_{67}$ MG

obtained from MD simulations with temperature are plotted. Interatomic distance is found to decrease for Cu–Cu pair and increase for Cu–Zr pair with decreasing temperature, respectively, as shown in Fig. 4. For Zr–Zr pair, identical behavior of variation in the interatomic distance with temperature as that of Cu–Cu pair has been observed. These results support the shifting of peaks for Cu–Cu, Cu–Zr, and Zr–Zr with temperature as shown in Fig. 3a-c.

The difference of the Cu–Cu, Cu–Zr, and Zr–Zr pPDFs causes the splitting of the first peak of the total PDF at 300 K represented in Fig. 2. From Fig. 2, it can be seen that in total PDF, splitting of the second peak begins at $1.42\sigma_1$ and $1.79\sigma_1$. $\sigma_1 = 3.05$ Å is the first peak position as shown in Fig. 2. The distances $r_{Cu–Cu}$, $r_{Cu–Zr}$, and $r_{Zr–Zr}$ are estimated from the first peak maxima of the $g_{ij}(r)$. At 300 K, the distance of $r_{Cu–Cu}$, $r_{Cu–Zr}$, and $r_{Zr–Zr}$ obtained from Fig. 3a-c is 2.51 Å, 2.79 Å, and 3.13 Å, respectively, which is in good agreement with the experimental data ($r_{CuCu} = 2.47$ Å, $r_{CuZr} = 2.85$ Å, and $r_{ZrZr} = 3.20$ Å) for the $Cu_{50}Zr_{50}$ MG [29]. Earlier reports [55, 56] have shown that the first peak position is mainly determined by the Zr–Zr partials in the Zr-rich liquids. The *R* values close to the Zr–Zr bond length corresponds to the Zr-rich liquid [57]. It appears that when the peak in g(r) is dominated by one of the partials, it follows the temperature dependence of those partials which can shift to the smaller/larger *R* with increasing/decreasing temperature. The relative growth rates and contributions of the partials may result in a contraction or expansion of the first shell [56]. In the present work, the value of peak position at 300 K obtained from MD simulations is 3.05 Å which is close to that of Zr–Zr partials. Therefore, it can be said that the total g(r) follows the temperature dependence of Zr–Zr partials.

Further, the splitting of the second peak was found to begin at an identical temperature of 300 K as observed in the $g_{Cu–Cu}(r)$ and $g_{Zr–Zr(r)}$ pPDFs, as displayed in Fig. 3a and Fig. 3c. Besides, the interatomic distances at which splitting of the second peak begins are also calculated. It was found that splitting has emerged at $1.83\sigma_1$ and $2.17\sigma_1$ for the Cu–Cu pairs and $1.78\sigma_3$ and $1.94\sigma_3$ for the Zr–Zr pairs, respectively, where $\sigma_1 = 2.51$ Å and $\sigma_3 = 3.13$ Å are the first peak position, respectively, in the Cu–Cu and Zr–Zr pPDFs. However, no splitting of the second peak for the Cu–Zr pair has been observed. Present calculations match well with available literature [29, 52, 58] and reflect the universality of PDFs in MGs. Table 1 shows that atomic distances Cu–Cu, Cu–Zr, and Zr–Zr are less than that of Goldsmith radius [44, 59] of the crystalline positions. It is known that when first neighbor distances are shorter than crystalline positions, the atoms in the short-range order (SRO) regime acquired the position with minimum local energy and stabilizes the glassy phase [60]. It shows that the present EAM interatomic potential [36] is suitable to explain the structure of $Cu_{33}Zr_{67}$ MG. Besides, small shoulder peaks

Table 1 Comparative analysis of interatomic distances R (Å) of Cu−Cu, Cu−Zr, Zr−Zr as obtained by MD simulations for the $Cu_{33}Zr_{67}$ glassy ribbons at 10 K, 50 K, 100 K, 150 K, 200 K, and 300 K

Temperature	Cu–Cu (Å)		Cu–Zr (Å)		Zr–Zr (Å)	
	MD simulations	$R_{i\text{-}j}$	MD simulations	$R_{i\text{-}j}$	MD simulations	$R_{i\text{-}j}$
10 K	2.49	2.56	2.81	2.88	3.09	3.21
50 K	2.52	2.56	2.81	2.88	3.10	3.21
100 K	2.49	2.56	2.79	2.88	3.10	3.21
150 K	2.52	2.56	2.79	2.88	3.11	3.21
200 K	2.51	2.56	2.79	2.88	3.13	3.21
300 K	2.51	2.56	2.79	2.88	3.13	3.21

$R_{i\text{-}j}$ = interatomic distances calculated from the interatomic radius of the individual element as given in [44, 59]

are found to grow between first and second peaks on right at 300 K onwards as shown in Fig. 3b and c for $g_{Cu–Zr}$ and $g_{Zr–Zr}$, respectively. With further decrease in temperature, the peak intensities of the right shoulder boost and split into two sub-peaks as shown in Fig. 3b thereby showing the initiation of the ordered structure. The growth of the right sub-peak becomes more pronounced with decreasing temperature thereby supporting the possibility of orientation in the ordered structure at the atomic scale. In an earlier report [60], it has been stated that such a bump might result from the presence of atoms between the first and second coordination shells during cooling. This suggests that some of the atoms move towards each other thereby pushing other atoms between the first and second neighbor distance in the SRO regime [60]. The splitting of the second peaks for the Cu–Cu and Zr–Zr pairs at lower temperature supports the formation of the $Cu_{33}Zr_{67}$ glass [41, 42]. The growth in the height of the two sub-peaks can be attributed to the atomic rearrangement during cooling. For Zr–Zr pair, the second peak shifts to the right with an increase in height during the cooling process with no splitting. This shows the different environments of the Cu and Zr atoms in the $Cu_{33}Zr_{67}$ glass.

Earlier, it was reported that the Cu–Zr system exhibits longer Zr–Zr bonds, intermediate Cu–Zr, and short Cu–Cu in the first coordinating shell [35, 52]. These observations are consistent with the present findings as shown in Table 1 and can be confirmed with those of $\sigma_1 = 2.51$ Å, $\sigma_2 = 2.79$ Å, and $\sigma_3 = 3.13$ Å. In addition to the first shell, longer-range pair correlations such as second and third atomic shells have also been analyzed. The substantial differences in the pPDFs $g_{Cu–Cu}(r)$, $g_{Cu–Zr}(r)$, and $g_{Zr–Zr(r)}$ between the liquid and glass states can be remarkably noticed as shown in Fig. 3a-c. The pPDFs in the liquid at 2500 K show a significant degree of similarity, while at 10 K, plots show distinct variation. It was observed that the second shell for Cu–Cu and Zr–Zr partials shows a large degree of peak splitting. On the other hand, the Cu–Zr partial shows a considerable difference when comparing the liquid to the glassy state with the splitting of the peak at the first minima as shown in Fig. 3b. Strong temperature

Table 2 Interatomic distances R (Å) at the first peak, second peak, and third peak for $Cu_{33}Zr_{67}$ MG

Temperature	First peak	Second peak		Third peak
		1st sub-peak	2nd sub-peak	
2500 K	2.95	5.5		NA
300 K	3.05	4.33	5.46	7.92
200 K	3.02	4.46	5.46	7.92
150 K	3.03	4.36	5.48	7.92
100 K	3.06	4.19	5.46	7.93
50 K	3.03	4.12	5.47	7.94
10 K	3.04	4.12	5.47	7.96

dependence of the separation of the peaks and their relative intensities has been observed as illustrated in Fig. 2 and Fig. 3a-c. The fluctuation in the height of the partial pairs beyond 7 Å is reasonably higher for the glass state. This shows the structural re-ordering of the glass in the second and third atomic shells [61]. Moreover, the interatomic distances of the second and third shells were found to shift to smaller R by lowering the temperature from 2500 to 10 K for Cu–Cu and Zr–Zr pair. On the other hand, these peaks were found to shift towards the higher R by lowering the temperature from 2500 to 10 K for Cu–Zr. These changes in the pPDFs show the variation in the atomic ordering up to 10 Å. This could be stated as the densification of the atomic packing by lowering the temperature [62]. The values of interatomic distances at the first peak, second peak, and third peak for $Cu_{33}Zr_{67}$, Cu–Cu, Cu–Zr, and Zr–Zr are given in Tables 2, 34 to 5, respectively. From Fig. 3a1−c1, it can be seen that the different directions of the growth of the first peaks are responsible for the splitting of the first peaks with decreasing temperature in total PDF as shown in Fig. 2. Based on the evolution trend of first and second peaks with varying cooling rates and cooling temperatures, Zhang et al. [41] have suggested that the splitting of the first and second peaks can be viewed as an embryonic form of the crystal peak. Zhang et al. [41], as shown in Fig. 5,

Table 3 Interatomic distances *R* (Å) at the first peak, second peak, and third peak for Cu−Cu

Temperature	First peak	Second peak		Third peak
		1st sub-peak	2nd sub-peak	
2500 K	2.48	5.05		7.92
300 K	2.51	4.59	5.44	7.84
200 K	2.51	4.58	5.39	7.83
150 K	2.52	4.52	5.39	7.78
100 K	2.49	4.55	5.41	7.84
50 K	2.52	4.54	5.41	7.84
10 K	2.49	4.55	5.42	7.90

Table 4 Interatomic distances *R* (Å) at the first peak, second peak, and third peak for Cu−Zr

Temperature	First peak	Second peak	Third peak
2500 K	2.73	5.77	NA
300 K	2.79	5.35	7.81
200 K	2.79	5.36	7.82
150 K	2.79	5.38	7.88
100 K	2.79	5.38	7.84
50 K	2.81	5.41	7.85
10 K	2.81	5.43	7.85

Table 5 Interatomic distances *R* (Å) at the first peak, second peak, and third peak for Zr−Zr

Temperature	First peak	Second peak		Third peak
		1st sub-peak	2nd sub-peak	
2500 K	3.12	5.77		NA
300 K	3.13	5.56	6.07	8.07
200 K	3.13	5.54	6.10	8.05
150 K	3.11	5.52	6.18	8.02
100 K	3.10	5.50	6.15	8.02
50 K	3.10	5.53	6.16	8.04
10 K	3.09	5.49	6.15	8.01

plotted the fraction of the crystal-like regions with the temperature at different cooling rates. Zhang et al. [41] have divided the region into three zones as shown in Fig. 5. As shown in Fig. 2, it can be concluded that the shoulder peaks between first and second peaks and two sub-peaks on the second peak support the presence of short- or medium-range ordered structures in $Cu_{33}Zr_{67}$ MG. With this consensus, it can be concluded that there is a formation of some short- to medium-range ordered structure at cryogenics which leads to the coexistence of the disordered and crystal-like structure.

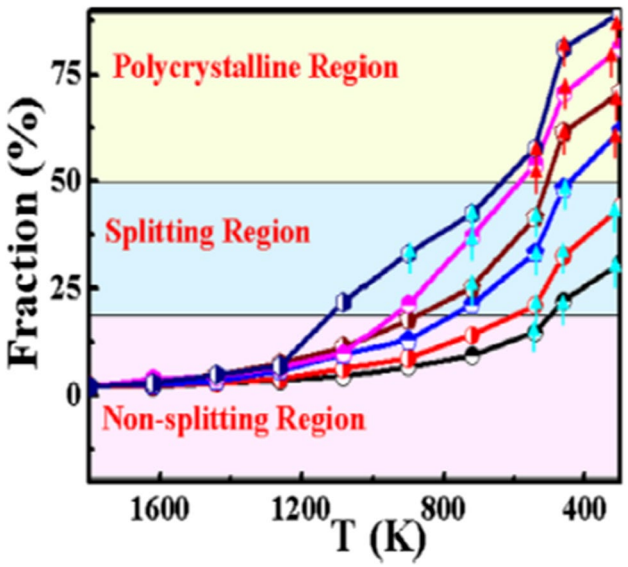

Fig. 5 Relationship between the fraction of the crystal-like region and the splitting of the second peak with different cooling rates: black line, 500 K/ps; red line, 250 K/ps; blue line, 100 K/ps; brown line, 50 K/ps; purple line, 25 K/ps; and dark blue line, 10 K/ps [41]. (Reproduced with permission from AIP Publishing House)

Proposed crystal structure evolution during cooling from 300 to 10 K

Wang et al. [63] have reported that the BMGs can be quenched compositionally neighboring the intermetallic compounds as close as 0.5 at.% [63]. Wang et al. [63] termed these BMG formers as "intermetallic glass" and showed that the liquid alloy neighboring the intermetallic compounds acquired lower Gibbs free energy compared to that of the compounds themselves [63, 64]. From the phase diagram as shown in Fig. 6 [63–65], it can be seen that the intermetallic phase $CuZr_2$ with tetragonal crystal structure exists near the same point where the glass-forming composition $Cu_{33}Zr_{67}$ is present. Therefore, it can be presumed that the low-temperature crystallization leads to the initiation of the development of the $CuZr_2$ phase. This can be presumed from the growth of the small peak between the first and second peaks of the total PDF of the $Cu_{33}Zr_{67}$ MG as seen in Fig. 2 and the presence of the crystal-like and disordered structural regions as seen in Fig. 4. Therefore, it could be suggested that the low-temperature treatment can be extended to the Cu–Zr binary MGs to improve the structural properties in addition to other reinforcement strategies [1, 6, 7].

Atomic-level structure analysis

From earlier reports [29, 52, 53, 62], it has been observed that the Voronoi cluster analysis is an effective way to identify the building units of atomic structures. Details about the

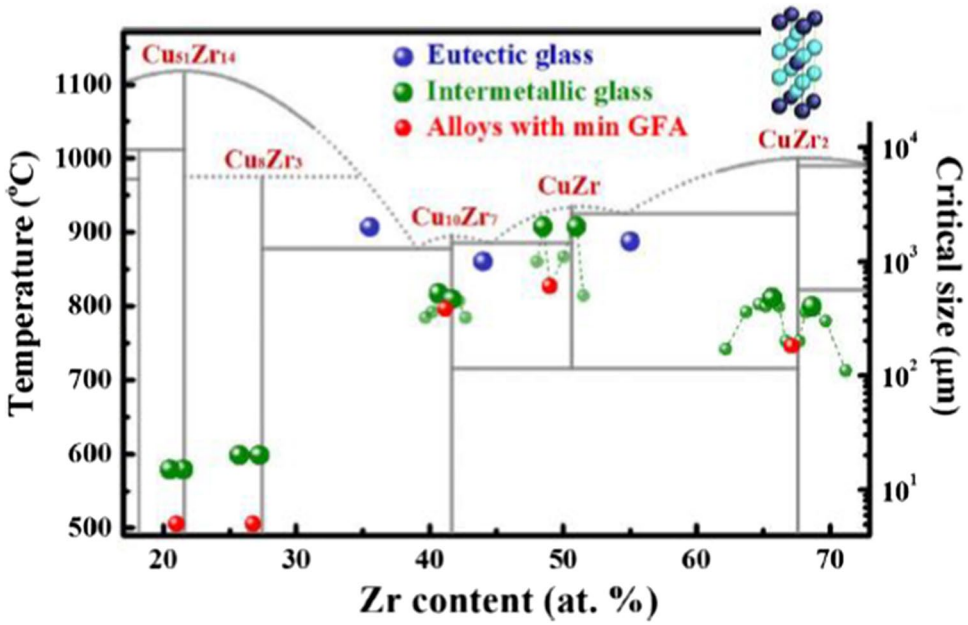

Fig. 6 Cu–Zr binary phase diagram, showing the evolution of critical sizes of intermetallic glass formers near each intermetallic compound, as well as the location of eutectic glass formers in the system with glass-forming rage [63]. (Reproduced with permission from ELSEVIER Publishing House)

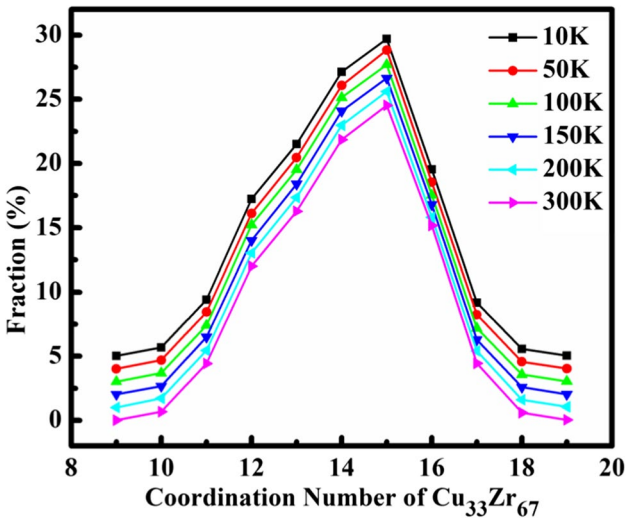

Fig. 7 Coordination number (CN) along with its corresponding population fraction for $Cu_{33}Zr_{67}$ MG at (a) 300 K, (b) 200 K, (c) 150 K, (d) 100 K, (e) 50 K, (f) 10 K, respectively

Voronoi tessellations can be found in [29, 52, 53]. Figure 7 shows the plots of coordination number (CN) for $Cu_{33}Zr_{67}$ MG at (a) 300 K, (b) 200 K, (c) 150 K, (d) 100 K, (e) 50 K, and (f) 10 K, respectively. From Fig. 7, it can be observed that at all studied temperatures CN = 15 has maximum population fraction followed by CN = 14, 13, 16, and 12. CN = 11 and 17 have low population fraction compared to them. From Table 6, it can be seen that with decreasing temperature from 300 to 10 K, the fraction of CN = 12–15 increases whereas the fraction of CN = 16–17 decreases. Moreover, a very small decrease in the fraction of CN = 11 has been observed. Table 6 shows that with lowering the temperature, the tendency of atomic configuration evolution increases by 0.22%, 25%, 0.29%, and 0.16%, respectively, for CN = 12, 13, 14, and 15. On the other hand, CN = 16 and 17 decrease by 0.64% and 0.26%, respectively. Therefore, the cluster evaluation in $Cu_{33}Zr_{67}$ can be ascribed as the coordinated clusters with CN 16 and 17 with a large bond length between center atoms, and the atoms in a shell declined into

Table 6 Variation in coordination number (CN) with its corresponding population fractions (%) for $Cu_{33}Zr_{67}$ MG at 300 K, 200 K, 150 K, 100 K, 50 K, 10 K

CN	2500 K	300 K	200 K	150 K	100 K	50 K	10 K
11	2.43	4.43	4.44	4.50	4.41	4.45	4.41
12	7.44	12.01	12.03	12.01	12.23	12.10	12.23
13	15.12	16.27	16.35	16.40	16.52	16.46	16.52
14	21.28	21.85	21.97	22.08	22.14	22.08	22.14
15	22.71	24.53	24.61	24.64	24.69	24.83	24.69
16	17.12	15.17	14.80	14.79	14.53	14.53	14.53
17	9.01	4.44	4.41	4.29	4.18	4.25	4.18
18	3.35	0.58	0.61	0.58	0.56	0.57	0.57

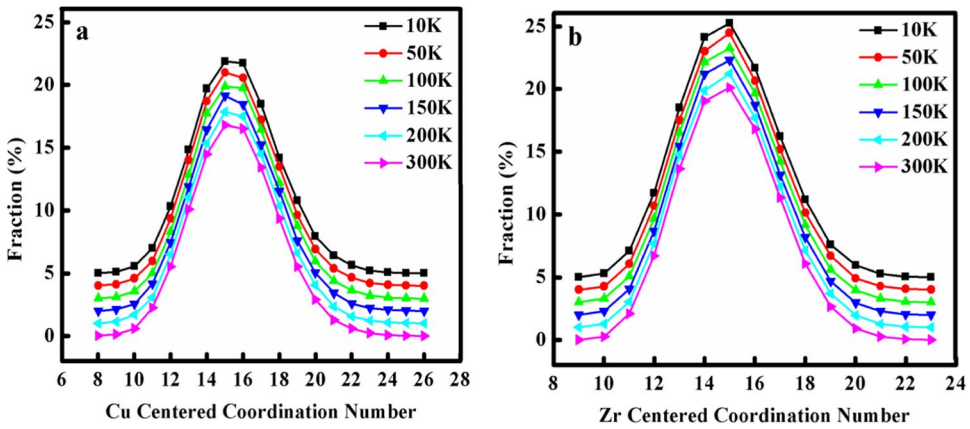

Fig. 8 Coordination number (CN) distribution around the **a** Cu and **b** Zr atoms, respectively, for $Cu_{33}Zr_{67}$ MG at 300 K, 200 K, 150 K, 100 K, 50 K, 10 K, respectively

Table 7 Variation in Voronoi polyhedra (VPs) (%) with its corresponding population fractions (%) for $Cu_{33}Zr_{67}$ MG at 300 K, 200 K, 150 K, 100 K, 50 K, 10 K

CN	VPs	10 K	50 K	100 K	150 K	200 K	300 K
10	<0280>	0.4	0.4	0.4	0.4	0.4	0.4
	<0361>	0.2	0.2	0.2	0.2	0.2	0.2
11	<0281>	2.4	2.4	2.4	2.3	2.3	2.2
	<0362>	0.4	0.4	0.4	0.4	0.4	0.4
	<0443>	0.4	0.5	0.5	0.5	0.4	0.5
12	<00,120>	0.8	0.7	0.8	0.8	0.7	0.7
	<0282>	3.3	3.2	3.2	3.2	3.1	3.0
	<0363>	2.5	2.3	2.4	2.3	2.3	2.3
	<0444>	1.0	1.1	1.1	1.1	1.1	1.1
	<0525>	0.3	0.3	0.3	0.2	0.3	0.3
13	<01,102>	1.8	1.8	1.8	1.7	1.7	1.7
	<0283>	0.9	0.9	0.9	0.8	0.9	0.8
	<0364>	4.8	4.7	4.8	4.6	4.5	4.4
	<0445>	1.3	1.2	1.2	1.3	1.2	1.2
	<0526>	0.7	0.7	0.7	0.7	0.7	0.7
14	<00,122>	0.5	0.4	0.5	0.5	0.4	0.4
	<01,103>	1.8	1.8	1.8	1.7	1.7	1.6
	<0284>	4.3	4.2	4.2	4.2	4.0	4.0
	<0365>	3.1	3.2	3.1	3.1	3.0	3.1
	<0383>	0.1	0.1	0.1	0.1	0.1	0.1
	<0446>	2.6	2.6	2.6	2.6	2.7	2.5
	<0464>	0.2	0.2	0.2	0.2	0.2	0.2
	<0608>	0.3	0.3	0.3	0.3	0.3	0.2
15	<01,104>	2.1	2.1	1.9	2.0	1.9	1.9
	<00,123>	0.4	0.3	0.4	0.4	0.3	0.3
	<0285>	3.6	3.6	3.5	3.4	3.4	3.2
	<0366>	3.1	3.1	3.2	3.1	3.0	3.0
	<0447>	1.7	1.7	1.7	1.7	1.6	1.7
	<0528>	0.2	0.2	0.2	0.2	0.2	0.2
16	<00,124>	0.1	0.1	0.1	0.1	0.1	0.1
	<01,105>	0.6	0.7	0.7	0.7	0.7	0.7
	<0286>	1.3	1.4	1.4	1.4	1.4	1.4
	<0367>	1.0	1.0	1.1	1.1	1.0	1.0
	<0448>	0.6	0.6	0.6	0.6	0.7	0.7
17	<01,106>	0.1	0.1	0.1	0.1	0.1	0.1
	<0287>	0.2	0.2	0.2	0.2	0.2	0.2
	<0368>	0.2	0.2	0.2	0.2	0.2	0.2
	<0449>	0.1	0.1	0.1	0.1	0.1	0.1

a coordinated cluster of CN with 12–15 with smaller bond lengths upon cooling [56]. It is known that the icosahedral cluster has 12 neighboring atoms and has a CN = 12 [66, 67]. The population fraction of atoms with CN = 12 for $Cu_{33}Zr_{67}$ was found to be constant throughout the temperature range of 10−300 K with a small variation of 0.1%. In the present investigation, CN analysis of $Cu_{33}Zr_{67}$ has shown the higher population fraction of CN = 12 at 10 K indicating the higher GFA of the specimen. Considering the Cu and Zr atoms as the center of the polyhedron, distribution of CN, and different Voronoi clusters (VC), analysis for the $Cu_{33}Zr_{67}$ MG at 300 K, 200 K, 150 K, 100 K, 50 K, and 10 K has been evaluated. Figure 8 shows the variation in Cu- and Zr-centered CN at various temperatures. From Fig. 8, it can be seen that CN = 15 and 16 are the most dominating at all temperatures centered on Cu and Zr atoms. Zr-centered polyhedra are mainly CNs with 13, 14, 15, 16, 17, and even 18 for liquid $Cu_{64}Zr_{36}$ and are decreased with further increasing Zr content [60]. The presence of Cu-centered CNs of 13 and 14 has also been expected in some BMGs [60, 68]. From the common neighbor analysis [60], it has been unfolded that the presence of complex geometries in Cu–Zr MG is a result of the packing among nearby atoms as well as related to the chemical bonding.

Hidden topological orders in $Cu_{33}Zr_{67}$ metallic glass

Different characteristic constant sequences correspond to the different lattice structures [42]. Henceforth, to understand the different topological ordering in the $Cu_{33}Zr_{67}$ MG, the scaled peak positions of the partial PDFs have been analyzed. Ratio R_i/R_1 ($i = 2,3,4$) in Cu–Cu pPDFs chooses the characteristic constants of the fcc lattice structure. For Cu–Zr pPDFs, it has been observed that the values of R_2/R_1 and R_3/R_1 follow bcc and fcc orders, respectively. Similar results were also observed in Zr–Zr partial PDFs. It has been observed that the R_2/R_1 and R_i/R_1 ($i = 3,4$) follow fcc order and bcc order, respectively. Hence, in Cu–Zr and Zr–Zr pPDFs, the hidden order follows both fcc order and bcc order. Thus, three different hidden orders are identified in

Table 8 Classification of VPs (%) based on Hwang [69] criteria for $Cu_{33}Zr_{67}$ glass

Types	VP	10 K	50 K	100 K	150 K	200 K	300 K
Perfect icosahedra	<00,120>	0.8	0.7	0.8	0.8	0.7	0.7
Quasi icosahedral	<01,102>	1.8	1.8	1.8	1.7	1.7	1.7
	<01,103>	1.8	1.8	1.8	1.7	1.7	1.6
	<01,104>	2.1	2.1	1.9	2.0	1.9	1.9
	<01,105>	0.6	0.7	0.7	0.7	0.7	0.7
	<01,106>	0.1	0.1	0.1	0.1	0.1	0.1
	<0281>	2.4	2.4	2.4	2.3	2.3	2.2
	<0282>	3.3	3.2	3.2	3.2	3.1	3.0
	<0283>	0.9	0.9	0.9	0.8	0.9	0.8
	<0284>	4.3	4.2	4.2	4.2	4.0	4.0
	<0285>	3.6	3.6	3.5	3.4	3.4	3.2
	<0286>	1.3	1.4	1.4	1.4	1.4	1.4
	<0287>	0.2	0.2	0.2	0.2	0.2	0.2
Mixed clusters	<0362>	0.4	0.4	0.4	0.4	0.4	0.4
	<0363>	2.5	2.3	2.4	2.3	2.3	2.3
	<0364>	4.8	4.7	4.8	4.6	4.5	4.4
	<0365>	3.1	3.2	3.1	3.1	3.0	3.1
	<0366>	3.1	3.1	3.2	3.1	3.0	3.0
	<0367>	1.0	1.0	1.1	1.1	1.0	1.0
	<0368>	0.2	0.2	0.2	0.2	0.2	0.2
Crystal-like clusters	<0443>	0.4	0.5	0.5	0.5	0.4	0.5
	<0444>	1.0	1.1	1.1	1.1	1.1	1.1
	<0445>	1.3	1.2	1.2	1.3	1.2	1.2
	<0446>	2.6	2.6	2.6	2.6	2.7	2.5
	<0447>	1.7	1.7	1.7	1.7	1.6	1.7
	<0448>	0.6	0.6	0.6	0.6	0.7	0.7
	<0449>	0.1	0.1	0.1	0.1	0.1	0.1
	<0525>	0.3	0.3	0.3	0.2	0.3	0.3
	<0526>	0.7	0.7	0.7	0.7	0.7	0.7

$Cu_{33}Zr_{67}$ glasses. Considering the present analysis, it can be stated that all three partial PDFs, as shown in Fig. 3a-c, are distinct indicating the different range of atomic packing orders in Cu–Cu, Cu–Zr, and Zr–Zr, respectively. The existence of different topological order in pPDFs can be attributed to the splitting of the first peak and second peak in total PDF as shown in Fig. 2. This analysis supports the good GFA of the Cu–Zr MGs in the present work.

Voronoi clusters (VC) in $Cu_{33}Zr_{67}$

Voronoi analysis has revealed that there are 38 VCs in the $Cu_{33}Zr_{67}$ MG having CN of 10–17 at the studied temperature range. From Table 7, it can be seen that the population of the VCs <0281>, <0282>, <0363>, <0364>, <0284>, <0365>, <0446> <01104>, <0285>, and <0366> was more than 2%. Besides, the population fraction of VCs <0444>, <01102>, <0445>, <01103>, <0447>, <0286>, and <0367> was in the range of 1 to 2%. Among them, <0364> was found to have a maximum population of 4.4% and 4.8% at 300 K and 10 K, respectively. On the other hand, <00124> <01106>, and <0449> were found to have the lowest population of 0.1% over the complete temperature range. A list of VCs over the temperature range can be found in Table 7. Further, these VCs have been classified into perfect icosahedra, quasi icosahedral, mixed-type clusters, and crystal-like clusters as proposed by Hwang [69] as listed in Table 8. Table 8 show that the quasi icosahedral VCs such as <01102>, <01103>, <01104>, <0281>, <0282>, <0284>, <0285>, and <0286>; mixed-type cluster such as <0363>, <0364>, <0365>, <0366>, and <0367>; and crystal-like cluster such as <0444>, <0445>, <0446>, and <0447> majorly contribute to the formation of the glass and the splitting of the peaks (first and second) for $Cu_{33}Zr_{67}$ with decreasing temperature. For the present investigation, VCs with a fraction of more than 1% are considered. From Table 8, it can be noticed that the population fraction of quasi icosahedral VCs such as <01102>, <01103>, <01104>, <0281>, <0282>, <0284>, and <0285> increases as the temperature decreases down to 10 K. Among them, <0284>, <0285>, and <0283> are the top VCs with maximum population fraction which increases with decreasing temperature. Similarly, it can be seen that the population fraction of the mixed-type clusters such as <0363>, <0364>, <0365>, and <0366> increases with decreasing temperature. However, <0364>, <0366>, and <0365> have large fraction compared to other VCs. Uneven rise and fall in the population fraction of these can be seen in Fig. 9. Besides, a crystal-like cluster such as <0445> and <0446> increases with lowering the temperature. However, <0446> has a large population fraction among other crystal-like VCs, and <0447> has the second largest population. Both the

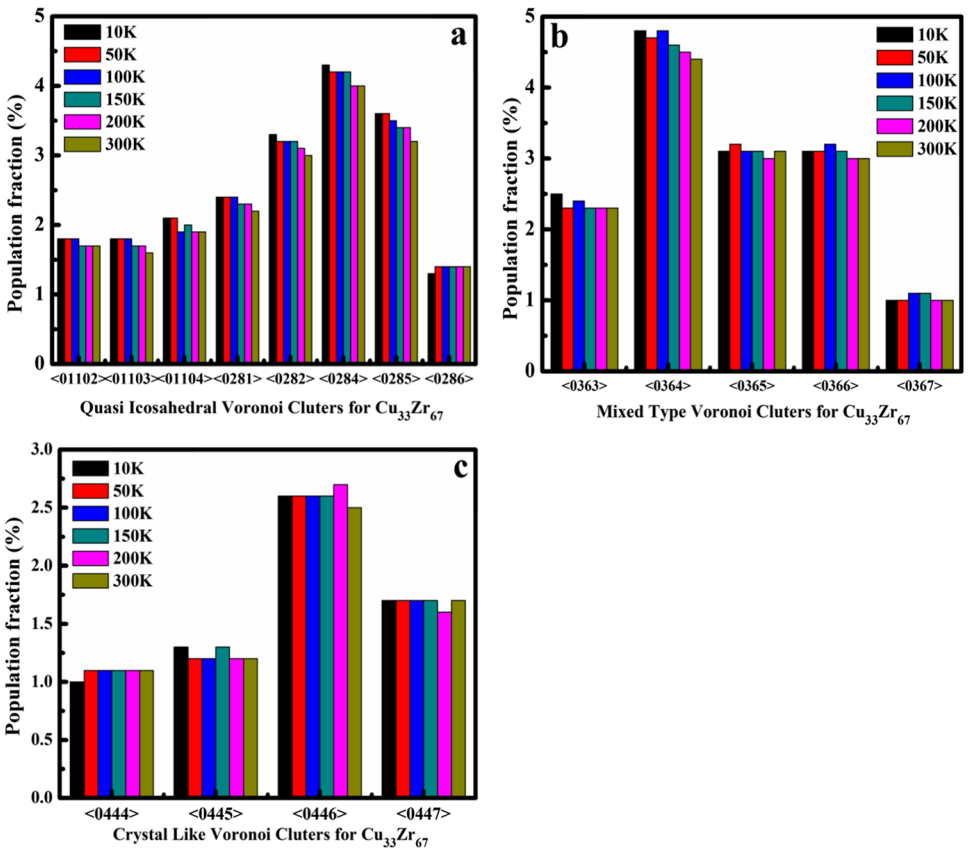

Fig. 9 Variation in population fraction (%) of **a** quasi icosahedral, **b** mixed-type, **c** crystal-like Voronoi clusters at 10 K, 50 K, 100 K, 150 K, 200 K, 300 K

Table 9 Classification of VPs (%) based on Hwang [69] criteria at Cu- and Zr-centered atoms for $Cu_{33}Zr_{67}$ MG

Types	VP	10K		50K		100K		150K		200K		300K	
		Cu	Zr	Cu	Zr	Cu	Zr	Cu	Zr	Cu	Zr	Cu	Zr
Perfect icosahedra	<00,120>	0	0.1	0	0.1	0	0.1	0	0.1	0	0	0	0.1
Quasi icosahedral	<01,103>	0	0.1	0	0.1	0	0.2	0	0.2	0	0.1	0	0.1
	<01,104>	0	0.1	0	0.1	0	0.2	0	0.2	0	0.1	0	0.1
	<01,105>	0.6	0.6	0.7	0.7	0.7	0.7	0.7	0.7	0.7	0.7	0.7	0.7
	<01,106>	0.1	0.1	0.1	0.1	0.1	0.1	0.1	0.1	0.1	0.1	0.1	0.1
	<0281>	0	0.3	0	0.4	0	0.4	0	0.4	0	0.4	0	0.4
	<0282>	0	0.7	0	0.6	0	0.7	0	0.7	0	0.7	0	0.7
	<0283>	0	0.5	0	0.5	0	0.5	0	0.5	0	0.4	0	0.4
	<0284>	0	0.7	0	0.6	0	0.6	0	0.6	0	0.6	0	0.6
	<0285>	0	0.3	0	0.3	0	0.3	0	0.3	0	0.3	0	0.3
	<0286>	1.3	1.3	1.4	1.4	1.4	1.4	1.4	1.4	1.4	1.4	1.4	1.4
	<0287>	0.2	0.2	0.2	0.2	0.2	0.2	0.2	0.2	0.2	0.2	0.2	0.2
Mixed clusters	<0361>	0	0.1	0	0.1	0	0.1	0	0.1	0	0.1	0	0.1
	<0362>	0.1	0.3	0	0.3	0	0.2	0	0.3	0	0.2	0	0.3
	<0363>	0.1	0.9	0.1	0.9	0.1	0.9	0.1	0.8	0.1	0.9	0.1	0.8
	<0364>	0.1	1.3	0.1	1.3	0.1	1.3	0.1	1.3	0.1	1.3	0.1	1.4
	<0365>	0.1	0.8	0	0.8	0.1	0.8	0.1	0.8	0.1	0.8	0.1	0.8
	<0366>	0.1	0.5	0.1	0.4	0.1	0.8	0.1	0.8	0.1	0.5	0.1	0.4
	<0367>	1.0	1.0	1.0	1.0	1.1	1.1	1.1	1.1	1.0	1.0	1.0	1.0
	<0368>	0.2	0.2	0.2	0.2	0.2	0.2	0.2	0.2	0.2	0.2	0.2	0.2
Crystal-like clusters	<0442>	0	0.1	0	0.1	0.1	0.1	0	0.1	0.1	0	0.1	0.1
	<0443>	0.1	0.4	0.1	0.3	0.1	0.3	0.1	0.4	0.1	0.4	0.1	0.4
	<0444>	0.1	0.5	0.1	0.6	0.1	0.5	0.1	0.6	0.1	0.5	0.1	0.5
	<0445>	0.1	0.5	0.1	0.5	0.1	0.6	0.1	0.6	0.1	0.6	0.1	0.6
	<0446>	0.1	0.6	0.1	0.5	0	0.6	0.1	0.6	0.1	0.5	0.1	0.5
	<0447>	0	0.3	0	0.2	0	0.2	0	0.2	0	0.2	0	0.2
	<0448>	0.6	0.6	0.6	0.6	0.6	0.6	0.6	0.6	0.7	0.7	0.7	0.7
	<0449>	0.1	0.1	0.1	0.1	0.1	0.1	0.1	0.1	0.1	0.1	0.1	0.1
	<0525>	0	0.1	0	0.1	0	0.1	0	0.1	0	0.1	0	0.1
	<0526>	0	0.1	0	0.1	0	0.1	0	0.1	0	0.1	0	0.1

VCs are found to have an almost constant population over the studied temperatures. Further, quasi icosahedral VC such as <0286> and mixed-type cluster such as <0367> were found to decrease with lowering temperature as can be seen from Table 8. Moreover, the population fraction of mixed-type clusters such as <0367> was found to increase first from 300 to 100 K and then decrease with a further fall of temperature from 100 to 10 K. Besides, crystal-like VC such as <0447> remains constant at all studied temperatures. However, the population fraction of the perfect icosahedra <00120> is almost constant (i.e., 0.7−0.8%) in the temperature range of 10−300 K. Therefore, in Fig. 8, only those VCs are plotted for which the population fraction is more than or equal to 1%.

Further, to clarify the role of both Cu- and Zr-centered polyhedral, VCs are classified into Cu-centered and Zr-centered as illustrated in Table 9. Figure 10a shows that Cu-centered quasi icosahedral VCs <0286> and <01105> are constant with decreasing temperature from 300 to 50 K and slightly decreased further at 10 K. Moreover, Zr quasi icosahedral VCs such as <0286>, <0282>, and <01105> are majorly contributing towards the glass formation in $Cu_{33}Zr_{67}$ as seen in Fig. 10b. It can be seen tha t <0286> and <01105> remain constant over the temperature range of 300 K to 50 K and decrease slightly at 10 K. Similarly, <0282> remains constant as the temperature decreases from 300 to 100 K and then attains a minimum at 50 K. Further, with a decrease in temperature down to 10 K, a population fraction of <0282> increases to its room temperature fraction. Figure 10c shows that <0367> has the highest population fraction of mixed-type VCs at Cu center compared to other VCs. It can be observed that the fraction of <0367> first increases and then decreases with lowering the temperature. At 100 K and150K, <0367> has the highest population fraction than other temperatures. From Fig. 10d, it can be seen that <0364>, <0367>, <0363>, and <0365> are the major mixed-type cluster at Zr center. Although a fraction of <0364> decreased at 200 K, it remains constant and maximum compared to other clusters. Similarly, the fraction of <0367> increases first and then

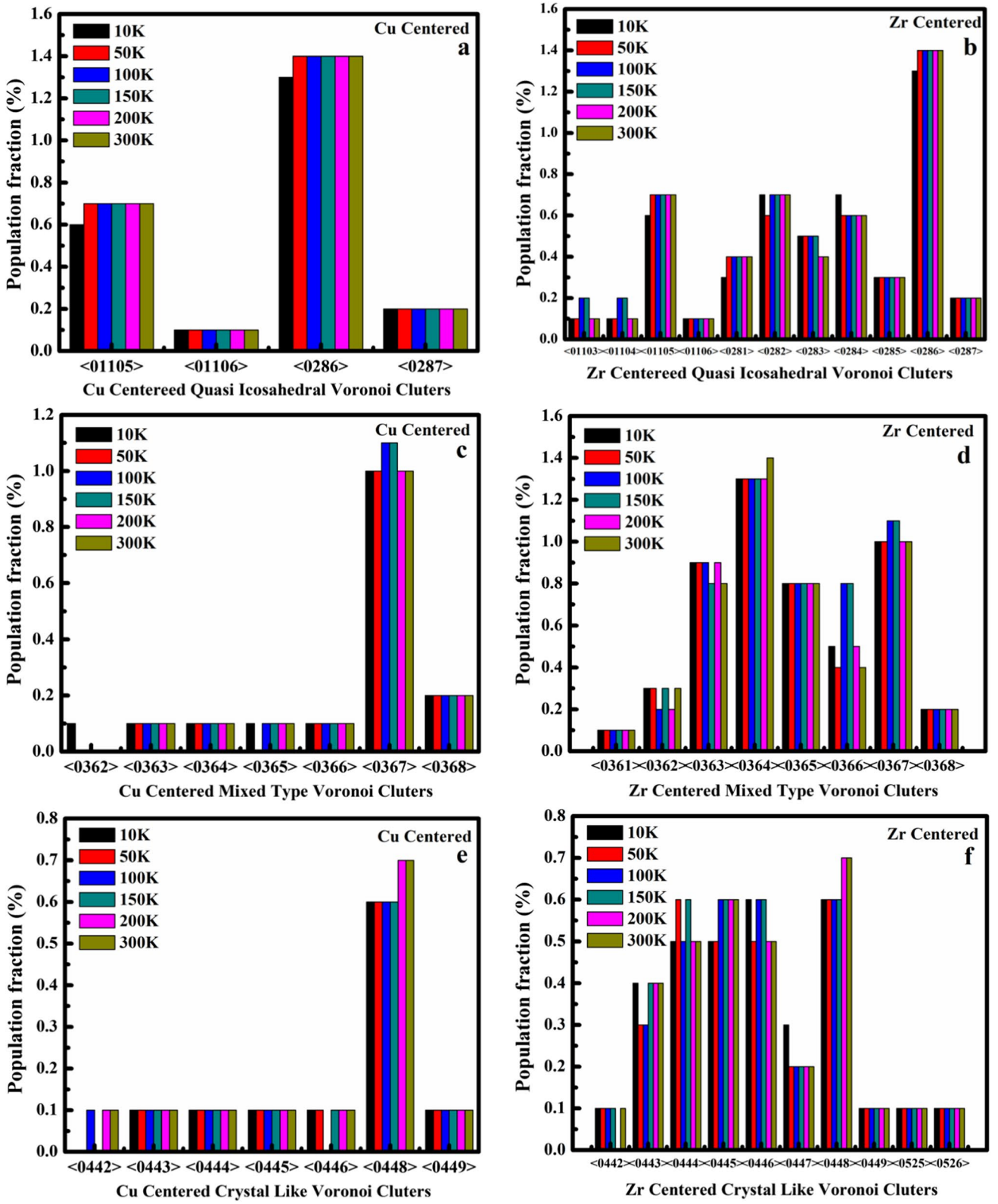

Fig. 10 **a** and **b** Quasi icosahedral-type Voronoi clusters at Cu- and Zr-centered atoms, **c** and **d** mixed-type Voronoi clusters at Cu- and Zr-centered atoms, **e** and **f** crystal-like Voronoi clusters at Cu- and Zr-centered atoms

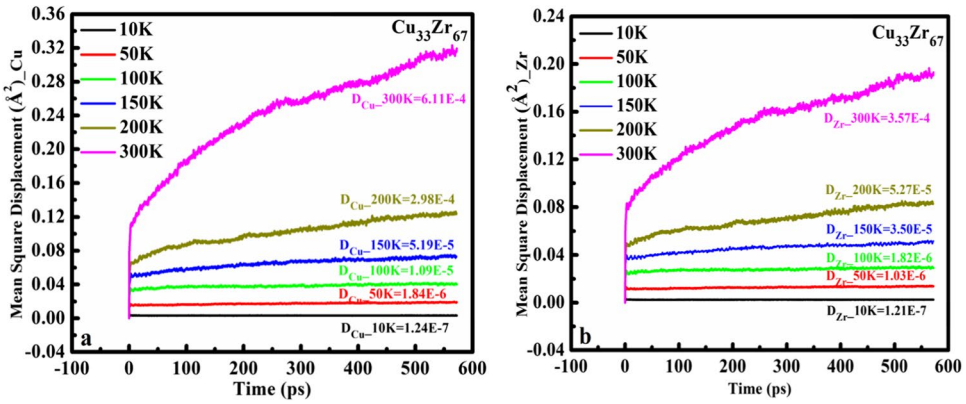

Fig. 11 Time dependence of the mean square displacement (MSD) for **a** Cu and **b** Zr atoms in the $Cu_{33}Zr_{67}$ MG at 10 K, 50 K, 100 K, 150 K, 200 K, 300 K

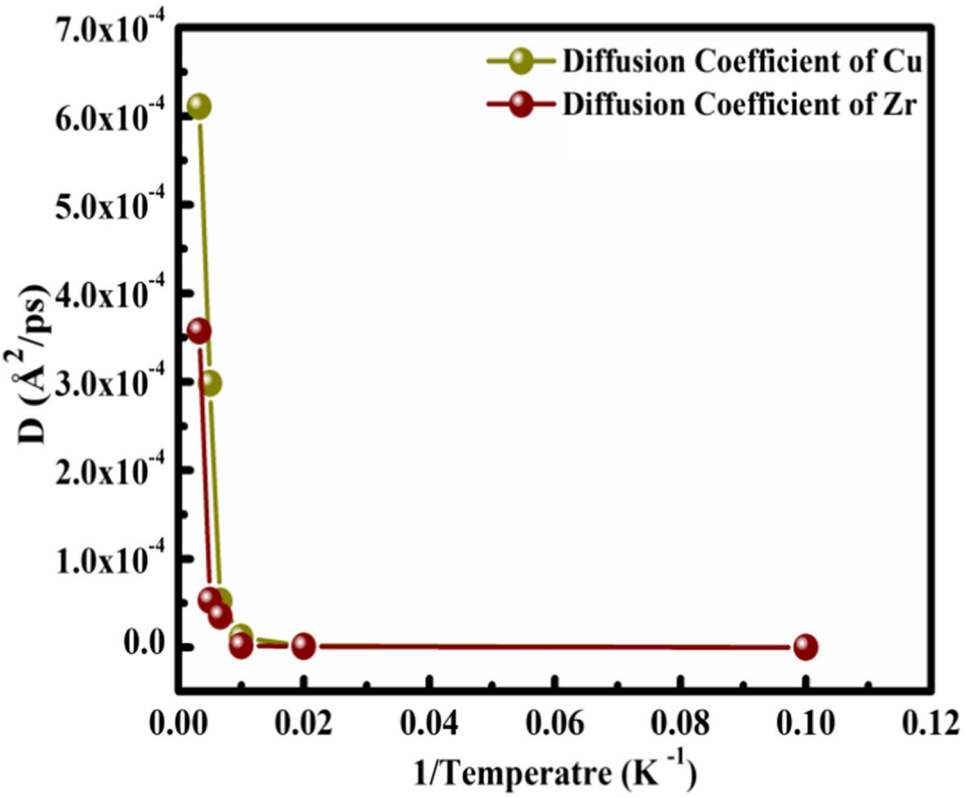

Fig. 12 Variation of the diffusion coefficient (D) for Cu and Zr atoms of the $Cu_{33}Zr_{67}$ MG

Table 10 Diffusion coefficient (D) of the Cu and Zr atom in the $Cu_{33}Zr_{67}$ MG at 10 K, 50 K, 100 K, 150 K, 200 K, and 300 K

Atom	10 K	50 K	100 K	150 K	200 K	300 K
Cu	1.24×10^{-7}	1.84×10^{-6}	1.09×10^{-5}	5.19×10^{-5}	2.98×10^{-4}	6.11×10^{-4}
Zr	1.21×10^{-7}	1.03×10^{-6}	1.82×10^{-6}	3.50×10^{-5}	5.27×10^{-5}	3.57×10^{-4}

D is in $Å^2/ps$

decreases as seen in Fig. 10d and remains the second largest population fraction of Zr-centered mixed-type VCs. From Fig. 10e, it can be seen that there is only one <0448> Cu-centered crystal-like VC with maximum population fraction compared to other VCs. It can be seen that at 150 K, population fraction decreases and remains constant throughout the temperature range. Four Zr-centered crystal-like VCs such as <0448>, <0445>, <0446>, and <0444> have been found with maximum population fraction at all studied temperatures compared to other VCs. It can be seen that

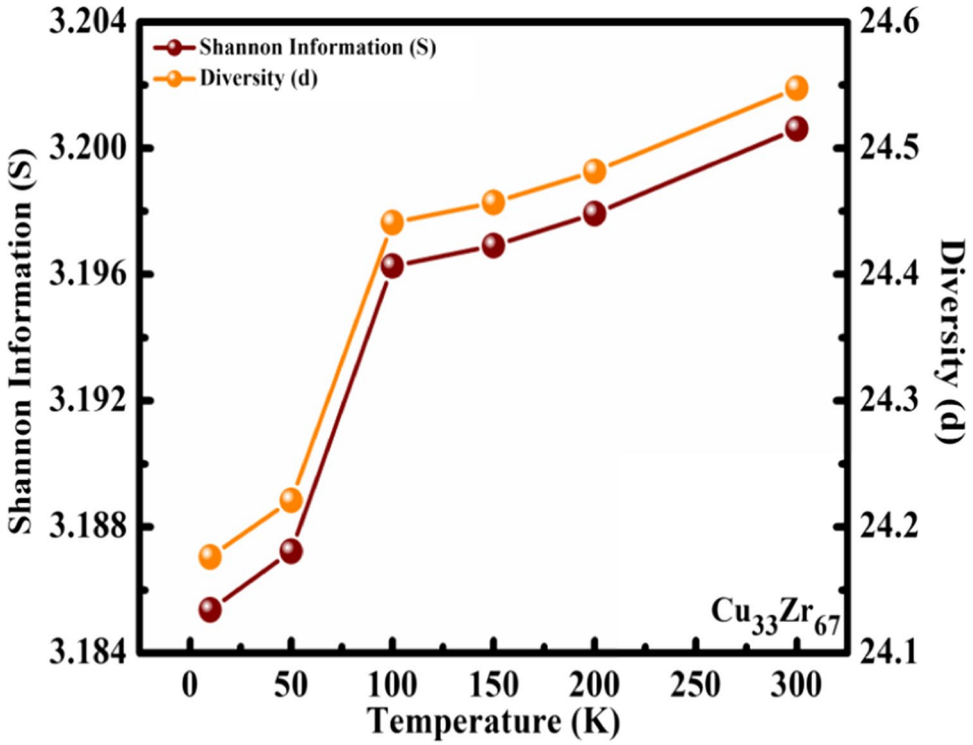

Fig. 13 Variation in Shannon information (*S*) and diversity (*d*) with temperature in $Cu_{33}Zr_{67}$ MGs

fraction of <0448> decreased at 150 K and remained constant over the temperature range of 150 to 10 K. Similarly, the population fraction of <0445> decreased at 100 K and remained constant up to 10 K. Besides, <0446> and <0444> show rise and fall of population fraction at different temperatures.

Mean square displacement (MSD)

The mean square displacement (MSD) of the Cu and Zr atoms has been calculated for the $Cu_{33}Zr_{67}$ metallic glass at different temperatures such as at 10 K, 50 K, 100 K, 150 K, 200 K, and300K. The variation of MSD for Cu and Zr atoms with time has been shown in Fig. 11. Typical behavior of the plots as reported by Sun et al. [43] for the $Cu_{60}Zr_{40}$ metallic glass can be viewed in Fig. 11 for both Cu and Zr atoms at 300 K, 200 K, and 150 K. Besides, MSD decreases sharply and remains almost constant at 100 K, 50 K, and 10 K, respectively, as seen from Fig. 11. The disappearance of the plateau below 150 K suggests that the atoms are trapped in the cages and no long-range diffusion has been obtained on the studied timescale. This can be evident from the calculation of the diffusion coefficient (*D*). Figure 12 shows the temperature dependence of the *D* for Cu as well as Zr atoms in the glassy state. It has been observed that *D* of Cu and Zr decreases as 1/T increased. This behavior is identical to that of $Cu_{60}Zr_{40}$ glass as reported by Sun et al. [43] thereby showing the universal behavior of the *D* for Cu and Zr, respectively. The diffusion coefficient of Cu was found to be more compared to that of Zr. It is due to the smaller atomic radius of the Cu (1.278 Å) compared to that of the Zr (1.603 Å) [44]. Numerical values of the diffusion coefficient (*D*) are given in Table 10. A non-Arrhenius behavior of the diffusivity with temperature has been evaluated. The diffusivity in the highly undercooled state is an important property to understand the phase competition, glass transition, and microstructural response corresponding to the different processing conditions and vitrification [70]. For Al–Sm glassy alloy, rapid growth of local clusters, i.e., short-range ordering (SRO), has been observed by Wang et al. [70]. Similar observations were noted for the $Al_{450}Sm_{50}$ by Sun et al. [71]. It is reported that these clusters are energetically favorable; therefore, it can be presumed that the atoms in these clusters could be less mobile and the rapid enhancement of SRO in the undercooled liquid state will slow down the dynamics making the deviation of the diffusivity from the Arrhenius equation [70]. Therefore, non-Arrhenius behavior of the diffusivity in the present work is likely caused by the local structural ordering as discussed in the PDF and pPDFs. This supports the present findings of the possibility of the evolution of the $CuZr_2$ structure at a lower temperature in the $Cu_{33}Zr_{67}$ glass.

Diversity(d) Considering the importance of the diversity (*d*) in the evolution of the structures in the metallic glasses [72, 73], in the present work, *d* is calculated for $Cu_{33}Zr_{67}$ MG at different temperatures. Mathematically, it can be expressed as [72, 73]

Table 11 Shannon information (S) and diversity (d) of $Cu_{33}Zr_{67}$ glass at different temperatures

Temperature (K)	Shannon information (S)	Diversity (d)
10	3.185	24.176
50	3.187	24.221
100	3.196	24.441
150	3197	24.457
200	3198	24.482
300	3.201	24.548

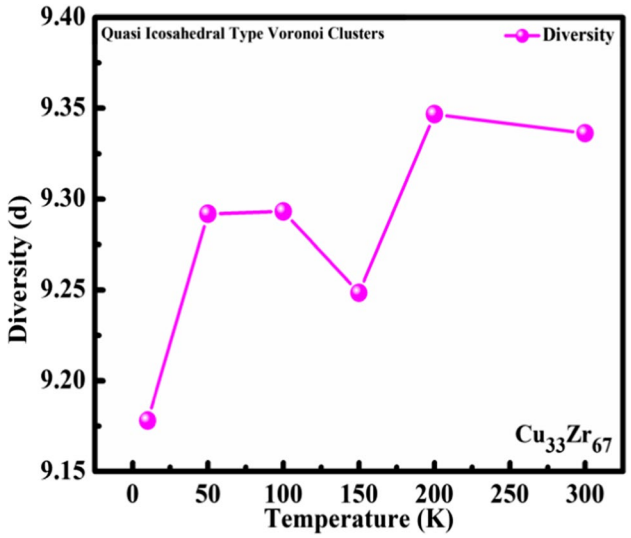

Fig.14 Variation in diversity (d) of quasi icosahedral-type Voronoi clusters with temperature in $Cu_{33}Zr_{67}$ MGs

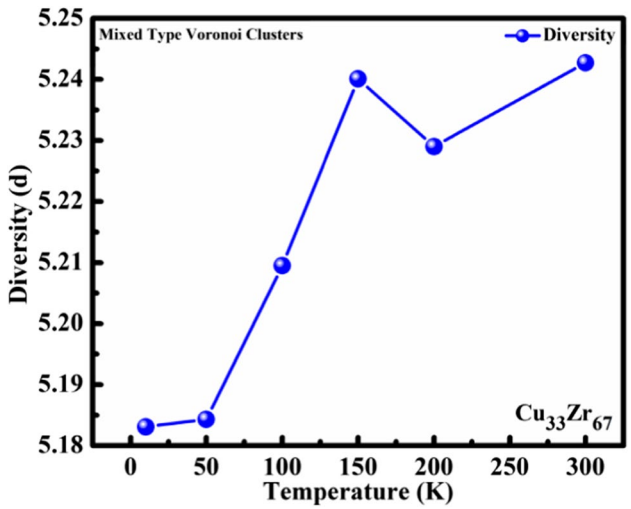

Fig. 15 Variation in diversity (d) of mixed-type Voronoi clusters with temperature in $Cu_{33}Zr_{67}$ MGs

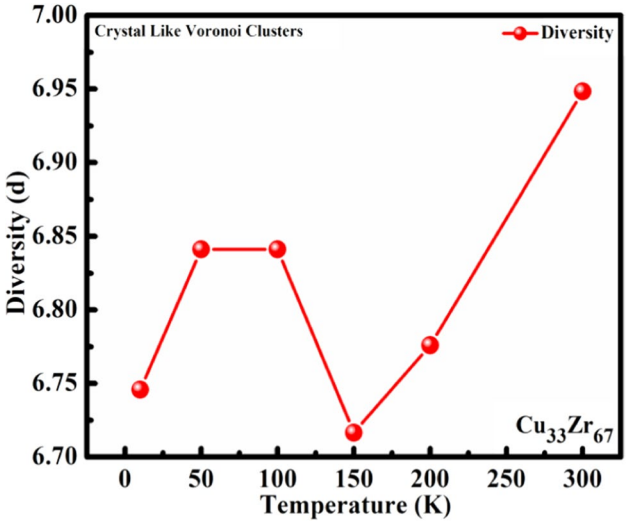

Fig. 16 Variation in diversity (d) of crystal-like Voronoi clusters with temperature in $Cu_{33}Zr_{67}$ MGs

Table 12 Diversity (d) of $Cu_{33}Zr_{67}$ glass for quasi icosahedral-type, mixed-type, and crystal-like clusters at different temperatures

Temperature (K)	Diversity (d)		
	Quasi icosahedral-type clusters	Mixed-type clusters	Crystal-like clusters
10	9.178	5.183	6.746
50	9.292	5.184	6.841
100	9.293	5.210	6.841
150	9.248	5.240	6.717
200	9.347	5.229	6.776
300	9.336	5.243	6.948

$$d = \exp(S) \tag{2}$$

$$S = -\sum_i p_i \ln p_i \tag{3}$$

In Eq. (3), S is the Shannon information and p_i is the fraction of Voronoi clusters.

Wei et al. [72] have considered $S = 0$ and $d = 1$ for the single local structure, i.e., perfect crystal structure. Statistical results have shown that $d > 100$ for glass-forming compositions and $d < 10$ for crystalline states. $10 < d < 100$ shows the intermediate structural diversities. In the present work, fraction p_i for each of the clusters has been calculated by normalizing the fractions given in Tables 7 to 9. For example, in Table 7, the addition of fractions of all clusters at 10 K was carried out, and then each of the fractions of the individual clusters was divided by the total sum. A similar approach was carried out for the rest of the calculations.

Shannon information (S) was calculated by putting these fractions in Eq. (3), and then diversity was calculated using Eq. (2). Figure 13 shows the variation in S and d as a function of temperature. This shows that with decreasing temperature from 300 to 10 K, S and d decrease reflecting the probability of the localization of the atoms. The numerical value of d ($10 < d < 100$), as shown in Table 11, reflects the presence of the intermediate structural diversities in $Cu_{33}Zr_{67}$ glass at the studied temperature ranges. Diversity was found to decrease by 40.2% from 300 to 10 K. These results support the reduction in the diffusion coefficient (D). Further, d was calculated for quasi icosahedral type, mixed-type, and crystal-like clusters as given in Table 8 to explore their role in the diversity of the glassy structure in $Cu_{33}Zr_{67}$ at low temperature.

Figure 14, Fig. 15, and Fig. 16 show the variation in diversity for quasi icosahedral-type, mixed-type, and crystal-like clusters with temperature. Numerical values given in Table 12 have shown that $d < 10$. From Table 12, it can be seen that there is a decrease in d by 15.8%, 6%, and 20.2% for quasi icosahedral-type, mixed-type, and crystal-like clusters, respectively. Among these clusters, mixed-type clusters have lower diversity favoring the formation of ordered structure. This result supports the probability of the embryonic development of the $CuZr_2$ phase in $Cu_{33}Zr_{67}$ at low temperatures as discussed in the section "Proposed crystal structure evolution during cooling from 300 to 10 K" and Fig. 5 and Fig. 6. Based on the Hwang [69] classification scheme, some of the VPs were omitted to calculate S and d at all studied temperatures. Therefore, some abrupt changes at 150 K in diversity have been observed for quasi icosahedral-type Voronoi clusters, mixed-type Voronoi clusters, and crystal-like Voronoi clusters in Fig. 14, Fig. 15, and Fig. 16, respectively. These VPs are <0280>, <0361>, <0383>, <0464>, <0528>, <0608>, <00,122>, <00,123>, and <00,124>. These VPS <0280>, <00,122>, <00,123>, <00,124>, and <0361> and <0383> have been classified into quasi icosahedral-type Voronoi clusters and mixed-type Voronoi clusters, respectively. Similarly, VPs <0464>, <0528>, and <0608> can be classified as crystal-like Voronoi clusters. S and d values of these VPs for each of these cluster type are calculated. For quasi icosahedral-type Voronoi clusters, S and d values are 1.09 and 2.97. For mixed-type Voronoi clusters, S and d are 0.35 and 1.42, respectively. Similarly, for crystal-like Voronoi clusters, S and d are 0.78 and 2.18, respectively. It is important to note that diversity (d) for quasi icosahedral-type Voronoi clusters and crystal-like Voronoi clusters is more than 2. Therefore, the omission of these VPs based on the Hwang [69] scheme has resulted in the drop in the d value at 150 K as can be seen from Fig. 14 and Fig. 16. However, for mixed-type Voronoi clusters, d is less than 1.5, and therefore small higher value is noticed as seen in Fig. 15. However, when these VPs are considered collectively as shown in Fig. 13, their individual characteristic gets disappeared and represents the average behavior for the system as a whole. From Fig. 17a, c and e, it can be seen that there is no conclusive trend in the diversity for quasi icosahedral-type, mixed-type, and crystal-like clusters at Cu-centered atoms. Diversity for quasi icosahedral-type cluster was found to remain constant over a temperature range from 300 to 50 K and suddenly attains its maximum at 10 k with an increase in d by 3%. Similarly, a linear decrease in d for mixed-type cluster was noticed from 300 to 50 K as shown in Fig. 17c which attained its maximum at 10 K with an increase of 65.9% in d. Besides, d remained constant from 300 to 200 K and dropped to its minimum by 21% at 150 K for crystal-like clusters. No change in the minimum value of d was further observed from 150 to 10 K as shown in Fig. 17e. Unlike Cu-centered cluster, a rise of 9.1%, 13%, and 23.1% was observed in d with decreasing temperature for Zr-centered quasi icosahedral-type, mixed-type, and crystal-like clusters as shown in Fig.17b, d and f. By analyzing different trends for d in Fig. 17 and numerical values in Table 13, it can be proposed that the decrease in d with temperature as observed in Fig. 13 to Fig. 16 is a collective behavior of low-diversity clusters such as Cu-centered quasi icosahedral clusters and Zr-centered mixed-type clusters.

Conclusions

In the present work, the dynamics of the structural evolution of the rapidly quenched $Cu_{33}Zr_{67}$ glass have been investigated by MD simulations at cryogenic temperatures 10–300 K. Splitting of the first and second peaks with decreasing temperature is found to be more pronounced. The presence of a shoulder on the high R side of the second peak has suggested the existence of the icosahedral short-range order (ISRO) in the $Cu_{33}Zr_{67}$ glass. A quasi-two-dimensional model supports the splitting of the first and second peaks in the $Cu_{33}Zr_{67}$. Zr−Zr pair is found responsible for the splitting of the first peak of the $Cu_{33}Zr_{67}$ glass at a lower temperature. The consensus of these observations has approved the validity of the EAM potentials used in the present work at cryogenics. Further, the Voronoi tessellation method has shown that quasi icosahedral such as <284>, <0285>, and <0282>; mixed-type cluster such as <0364>; and crystal-like cluster such as <0446> are responsible for the stabilization of the present glassy phase in the $Cu_{33}Zr_{67}$ glass. On the other hand, Cu-centered and Zr-centered <0286> quasi icosahedral VC has maximum population fraction

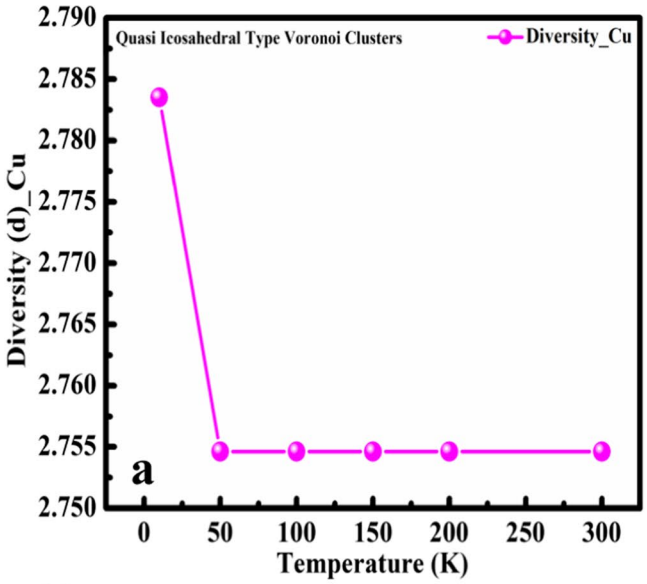
Quasi Icosahedral Type Voronoi Clusters
Diversity_Cu
Diversity (d)_Cu
Temperature (K)
a

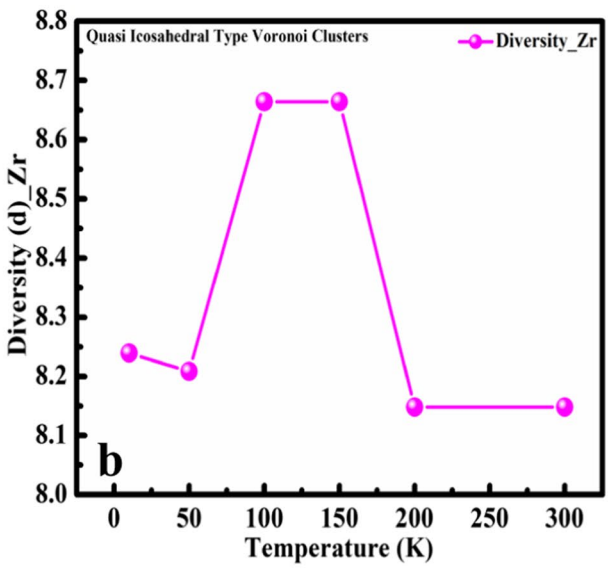
Quasi Icosahedral Type Voronoi Clusters
Diversity_Zr
Diversity (d)_Zr
Temperature (K)
b

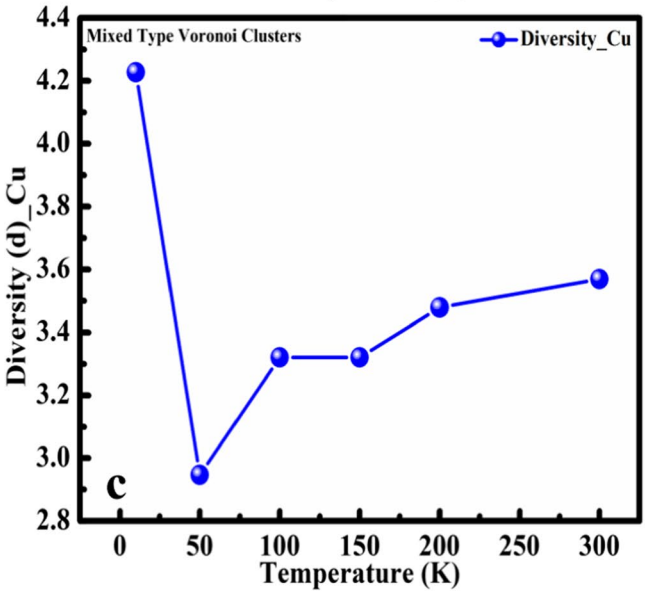
Mixed Type Voronoi Clusters
Diversity_Cu
Diversity (d)_Cu
Temperature (K)
c

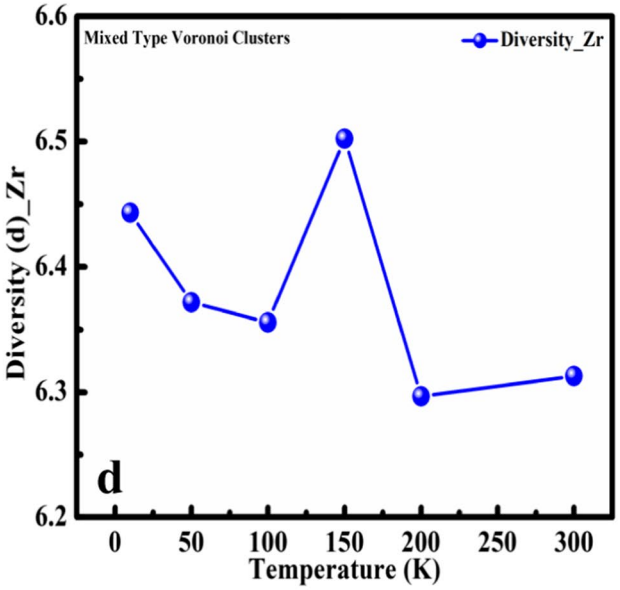
Mixed Type Voronoi Clusters
Diversity_Zr
Diversity (d)_Zr
Temperature (K)
d

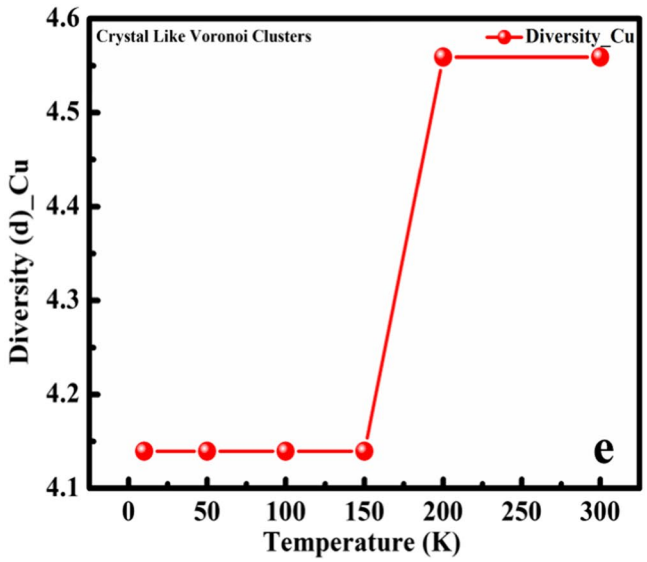
Crystal Like Voronoi Clusters
Diversity_Cu
Diversity (d)_Cu
Temperature (K)
e

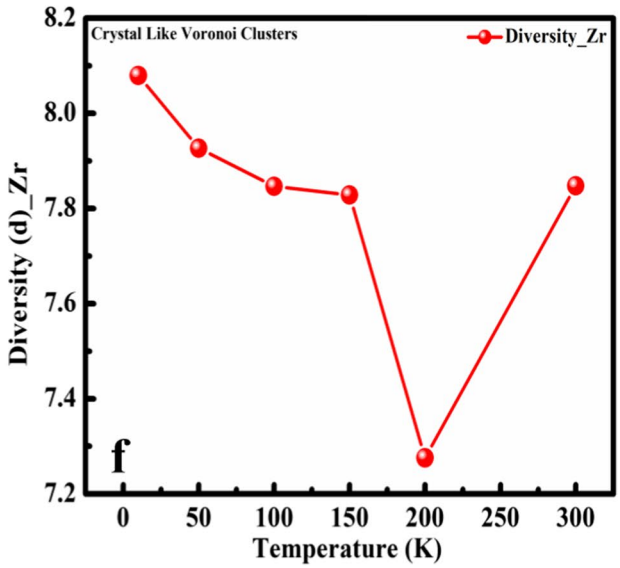
Crystal Like Voronoi Clusters
Diversity_Zr
Diversity (d)_Zr
Temperature (K)
f

◂**Fig. 17** Variation in diversity (d) in **a** and **b** quasi icosahedral-type Voronoi clusters at Cu- and Zr-centered atoms, **c** and **d** mixed-type Voronoi clusters at Cu- and Zr-centered atoms, **e** and **f** crystal-like Voronoi clusters at Cu- and Zr-centered atom with temperature

thereby supporting the stability of the glassy phase over the studied temperature range. Besides, the maximum population fraction of Cu-centered $<0367>$ and Zr-centered $<0364>$, $<0367>$, $<0363>$, and $<0365>$ mixed-type clusters and Cu-centered $<0448>$ and Zr-centered $<0448>$, $<0445>$, $<0446>$, and $<0444>$ crystal-like clusters support the possibility of the presence of intermediate phase of $CuZr_2$ at lower temperatures as observed from MD simulations. Relatively high atomic packing efficiency in the Zr-centered clusters has been identified in the $Cu_{33}Zr_{67}$ glass, and these compact clusters possess the local highest regularity, contributing to the stability of this glass. Further, mean square displacement (MSD) studies have shown that the diffusion coefficient of both Cu and Zr decreases with that of temperature. A smaller atomic radius provides a higher diffusion coefficient of the Cu compared to that of the Zr. Reduction in diversity with temperature has been noticed. A decrease in d is found to be the collective behavior of low-diversity clusters such as Cu-centered quasi icosahedral clusters and Zr-centered mixed-type clusters. The present MD simulations have provided the pathway for the critical evolution of the structural dynamics of the Cu–Zr metallic glass at cryogenic temperatures.

Acknowledgements Authors (A. A. Deshmukh, S. Pal) are thankful to the Department of Metallurgical and Materials Engineering, National Institute of Technology Rourkela, for providing the high-performance computational facilities to carry out these computational simulations.

Author contribution All the authors are actively involved in conceptualization; data curation; formal analysis; investigation; methodology; resources; software; supervision; validation; visualization; writing—original manuscript draft; and writing—review and editing.

Data availability The data that support the findings of this study are available from the corresponding author upon reasonable request.

Code availability On reasonable request, it will be available.

Declarations

Competing interests The authors declare no competing interests.

References

1. Parsapour H, Ajori S, Ansari R (2021) A molecular dynamics study on the tensile characteristics of various metallic glass nanocomposites reinforced by Weyl semimetals three-dimensional graphene network. Eur J Mech A Solids 85:104104. https://doi.org/10.1016/j.euromechsol.2020.104104
2. Suryanarayana C, Inoue A (2011) Bulk metallic glasses. CRC Press, Boca Raton, FL
3. Sharma S, Chandra R, Kumar P, Kumar N (2014) Effect of Stone-Wales and vacancy defects on elastic moduli of carbon nanotubes and their composites using molecular dynamics simulation. Comp Mater Sci 86:1–8. https://doi.org/10.1016/j.commatsci.2014.01.035
4. Sharma S, Chandra R, Kumar P, Kumar N (2016) Mechanical properties of carbon nanofiber reinforced polymer composites-molecular dynamics approach. JOM 68:1717–1727. https://doi.org/10.1007/s11837-016-1933-y
5. Sharma S, Kumar P, Chandra R (2016) Graphene/carbon nanotube reinforced metallic glass composites: a molecular dynamics study. Int J Multiscale Comput Eng 14:555–584. https://doi.org/10.1615/IntJMultCompEng.2016018635
6. Ajori S, Parsapour H, Ansari R, Ameri A (2019) Buckling behavior of various metallic glass nanocomposites reinforced by carbon nanotube and Cu nanowire: a molecular dynamics simulation study. Mater Res Express 6:095070. https://doi.org/10.1088/2053-1591/ab2cfd
7. Ajori S, Parsapour H, Ansari R (2020) A comprehensive analysis of the mechanical properties and fracture analysis of metallic glass nanocomposites reinforced by carbon nanotubes and Cu nanowires: a molecular dynamics study, Mech. Adv. Mater. Struct. 1-20https://doi.org/10.1080/15376494.2020.1746447
8. Yi J, Seifi SM, Wang W, Lewandowski JJ (2014) A damage-tolerant bulk metallic glass at liquid-nitrogen temperature. J Mater Sci Technol 30:627–630. https://doi.org/10.1016/j.jmst.2014.04.017
9. Fan C, Li H, Kecskes LJ, Tao K, Choo H, Liaw PK, Liu CT (2006) Mechanical behavior of bulk amorphous alloys reinforced by ductile particles at cryogenic temperatures. Phys Rev Lett 96:145506. https://doi.org/10.1103/PhysRevLett.96.145506

Table 13 Diversity (d) of $Cu_{33}Zr_{67}$ glass at Cu-centered and Zr-centered atoms for quasi icosahedral-type, mixed-type, and crystal-like clusters at different temperatures

Temperature (K)	Diversity (d)					
	Quasi icosahedral-type clusters		Mixed-type clusters		Crystal-like clusters	
	Cu	**Zr**	**Cu**	**Zr**	**Cu**	**Zr**
10	2.784	8.239	4.228	6.443	4.139	8.079
50	2.755	8.208	2.946	6.372	4.139	7.926
100	2.755	8.664	3.320	6.356	4.139	7.847
150	2.755	8.664	3.320	6.502	4.139	7.828
200	2.755	8.148	3.479	6.297	4.559	7.256
300	2.755	8.148	3.569	6.313	4.559	7.848

10. Stolyarov VV, Valiev RZ, Zhu YT (2006) Enhanced low-temperature impact toughness of nanostructured Ti. Appl Phys Lett 88:041905. https://doi.org/10.1063/1.2167800
11. Pan D, Guo H, Zhang W, Inoue A, Chen MW (2011) Temperature-induced anomalous brittle-to-ductile transition of bulk metallic glasses. Appl Phys Lett 99:241907. https://doi.org/10.1063/1.3669508
12. Yoon KS, Lee M, Fleury E, Lee JC (2010) Cryogenic temperature plasticity of a bulk amorphous alloy. Acta Mater 58:5295–5304. https://doi.org/10.1016/j.actamat.2010.06.002
13. Torre FHD, Klaumünzer D, Maaß R, Löffler JF (2010) Stick–slip behavior of serrated flow during inhomogeneous deformation of bulk metallic glasses. Acta Mater 58:3742–3750. https://doi.org/10.1016/j.actamat.2010.03.011
14. Sun BA, Pauly S, Hu J, Wang WH, Kühn U, Eckert J (2013) Origin of intermittent plastic flow and instability of shear band sliding in bulk metallic glasses. Phys Rev Lett 110:225501. https://doi.org/10.1103/PhysRevLett.110.225501
15. Griner S, Babilas R, Nowosielski R (2012) Structure and properties changes of $Fe_{78}Si_9B_{13}$ metallic glass by low temperature thermal activation process. J. Achiev. Mater. Manuf. Eng. 50(18):25 (http://jamme.acmsse.h2.pl/papers_vol50_1/5012.pdf)
16. Lesz S (2017) Effect of cooling rates on the structure, density and micro-indentation behavior of the Fe, Co-based bulk metallic glass. Mater Charac 124:97–106. https://doi.org/10.1016/j.matchar.2016.12.016
17. Dong C, Wang Q, Qiang JB, Wang YM, Jiang N, Han G, Li YH, Wu J, Xia JH (2007) From clusters to phase diagrams: composition rules of quasicrystals and bulk metallic glasses. J Phys D: Appl Phys 40:R273–R291. https://doi.org/10.1088/0022-3727/40/15/R01
18. Antonowicz J, Pietnoczka A, Drobiazg T, Almyras GA, Papageorgiou DG, Evangelakis GA (2012) Icosahedral order in Cu-Zr amorphous alloys studied by means of X-ray absorption fine structure and molecular dynamics simulations. Philos Mag 92:1865–1875. https://doi.org/10.1080/14786435.2012.659008
19. Wang CC, Wong CH (2012) Interpenetrating networks in Zr-Cu-Al and Zr-Cu metallic glasses. Intermetallics 22:13–16. https://doi.org/10.1016/j.intermet.2011.10.022
20. Cheng YQ, Ma E (2008) Indicators of internal structural states for metallic glasses: local order, free volume, and configurational potential energy. Appl Phys Lett 93:051910. https://doi.org/10.1063/1.2966154
21. Cheng YQ, Sheng HW, Ma E (2008) Relationship between structure, dynamics, and mechanical properties in metallic glass-forming alloys. Phys Rev B 78:014207. https://doi.org/10.1103/PhysRevB.78.014207
22. Dutta A (2018) Surface damage of CuZr metallic glass by hypervelocity nano-projectile: a molecular dynamics study. Comput Mater Sci 141:41–48. https://doi.org/10.1016/j.commatsci.2017.09.019
23. Sun P, Peng C, Cheng Y, Zhang G, Wang P, Jia L, Wang L (2019) Mechanical behavior of CuZr dual-phase nanocrystal-metallic glass composites. Comput Mater Sci 163:290–300. https://doi.org/10.1016/j.commatsci.2019.03.046
24. Amigo N, Urbina F, Valencia F (2020) Shear transformation zones structure characterization in $Cu_{50}Zr_{50}$ metallic glasses under tensile test. Comput Mater Sci 184:109941. https://doi.org/10.1016/j.commatsci.2020.109941
25. Wang P, Yang X (2020) Atomistic investigation of aging and rejuvenation in CuZr metallic glass under cyclic loading. Comput Mater Sci 185:109965. https://doi.org/10.1016/j.commatsci.2020.109965
26. Wu Y, Wang H, Wu HH, Zhang ZY, Hui XD, Chen GL, Ma D, Wang XL, Lu ZP (2011) Formation of Cu–Zr–Al bulk metallic glass composites with improved tensile properties. Acta Mater 59:2928–2936. https://doi.org/10.1016/j.actamat.2011.01.029
27. Liu Z, Li R, Liu G, Su WH, Wang H, Li Y, Shi MJ, Luo XK (2012) Microstructural tailoring and improvement of mechanical properties in CuZr-based bulk metallic glass composites. Acta Mater 60:3128–3139. https://doi.org/10.1016/j.actamat.2012.02.017
28. Ding J, Liu Z, Wang H, Zhang T (2014) Large-sized CuZr-based bulk metallic glass composite with enhanced mechanical properties. J Mater Sci Technol 30:590–594. https://doi.org/10.1016/j.jmst.2014.01.014
29. Li F, Liu XJ, Lu ZP (2014) Atomic structural evolution during glass formation of a Cu–Zr binary metallic glass. Comput Mater Sci 85:147–153. https://doi.org/10.1016/j.commatsci.2013.12.058
30. Ward L, Miracle D, Wind W, Senkov ON, Flores K (2013) Structural evolution and kinetics in Cu-Zr metallic liquids from molecular dynamics simulations. Phys Rev B 88:134205. https://doi.org/10.1103/PhysRevB.88.134205
31. Kluge M, Schober HR (2004) Diffusion and jump-length distribution in liquid and amorphous $Cu_{33}Zr_{67}$. Phys Rev B 70:224209. https://doi.org/10.1103/PhysRevB.70.224209
32. Kluge M, Schober HR (2006) Diffusion in a binary amorphous metal: Pair-correlation in $Cu_{33}Zr_{67}$. J Non-Cryst Solids 352:5093–5097. https://doi.org/10.1016/j.jnoncrysol.2006.01.155
33. Han XJ, Schober HR (2011) Transport properties and Stokes-Einstein relation in a computer-simulated glass-forming $Cu_{33.3}Zr_{66.7}$ melt. Phys Rev B 83:224201. https://doi.org/10.1103/PhysRevB.83.224201
34. Liu XJ, Wang SD, Fan HY, Ye YF, Wang H, Wu Y, Lu ZP (2018) Static atomic-scale structural heterogeneity and its effects on glass formation and dynamics of metallic glasses. Intermetallics 101:133–143. https://doi.org/10.1016/j.intermet.2018.08.001
35. Plimpton S (1995) Fast parallel algorithms for short-range molecular dynamics. J Comput Phys 117:1–119. https://doi.org/10.1006/jcph.1995.1039
36. Mendelev MI, Kramer MJ, Ott RT, Sordelet DJ, Yagodin D, Popel P (2009) Development of suitable interatomic potentials for simulation of liquid and amorphous Cu–Zr alloys. Philos Mag 89:967–987. https://doi.org/10.1080/14786430902832773
37. Li F, Zhang H, Liu X, Yu C, Lu Z (2018) Effects of cooling rate on the atomic structure of $Cu_{64}Zr_{36}$ binary metallic glass. Comp Mater Sci 141:59–67. https://doi.org/10.1016/j.commatsci.2017.09.026
38. Martyna GJ, Klein ML, Tuckerman M (1992) Nosé-Hoover chains: the canonical ensemble via continuous dynamics. J Chem Phys 97:2635–2643. https://doi.org/10.1063/1.463940
39. Reddy KV, Pal S (2019) Evaluation of glass forming ability of Zr–Nb alloy systems through liquid fragility and Voronoi cluster analysis. Comput Mater Sci 158:324–332. https://doi.org/10.1016/j.commatsci.2018.11.045
40. Pan SP, Feng SD, Qiao JW, Wang WM, Qin JY (2016) Correlation between local structure and dynamic heterogeneity in a metallic glass-forming liquid. J Alloys Compd 664:65–70. https://doi.org/10.1016/j.jallcom.2015.12.223
41. Zhang K, Li H, Li L, Bian XF (2013) Why does the second peak of pair correlation functions split in quasi-two-dimensional disordered films? Appl Phys Lett 102:071907. https://doi.org/10.1063/1.4793187
42. Wu ZW, Li MZ, Wang WH, Liu KX (2015) Hidden topological order and its correlation with glass-forming ability in metallic glasses. Nat Commun 6:6035. https://doi.org/10.1038/ncomms7035
43. Sun YL, Shen J, Valladares AA (2009) Atomic structure and diffusion in $Cu_{60}Zr_{40}$ metallic liquid and glass: molecular dynamics simulations. J Appl Phys 106:073520. https://doi.org/10.1063/1.3245324

44. Sheng G, Liu CT (2011) Phase stability in high entropy alloys: formation of solid-solution phase or amorphous phase. Prog Nat Sci Mater Int 21:433–446. https://doi.org/10.1016/S1002-0071(12)60080-X
45. Wang J, Hodgson PD, Zhang J, Yan W, Yang C (2009) Effects of quenching rate on amorphous structures of $Cu_{46}Zr_{54}$ metallic glass. J Mater Process Technol 209:4601–4606. https://doi.org/10.1016/j.jmatprotec.2008.10.048
46. Dalgic SS, Celtek M (2011) Liquid-to-glass transition in bulk glass-forming $Cu_{55-x}Zr_{45}Ag_x$ alloys using molecular dynamic simulations. EPJ Web of Conferences 15:03009. https://doi.org/10.1051/epjconf/20111503009
47. Lindwall J (2019) Modelling of bulk metallic glass formation in powder bed fusion. Licentiate Thesis. Lulea University of Technology, Lulea, Sweden
48. Lu Y, Zhang H, Li H, Xu H, Huang G, Qin Z, Lu X (2017) Crystallization prediction on laser three-dimensional printing of Zr-based bulk metallic glass. J Non-Cryst Solids 46:12–17. https://doi.org/10.1016/j.jnoncrysol.2017.01.038
49. Schroers J, Masuhr A, Johnson WL, Busch R (1999) Pronounced asymmetry in the crystallization behavior during constant heating and cooling of a bulk metallic glass-forming liquid. Phy Rev B 60:11855. https://doi.org/10.1103/PhysRevB.60.11855
50. Li F, Liu XJ, Hou HY, Chen G, Chen GL (2011) Atomic-scale structural evolution from disorder to order in an amorphous metal. J Appl Phys 110:123508. https://doi.org/10.1063/1.3669450
51. Durandurdu M (2012) Ab initio modeling of metallic $Pd_{80}Si_{20}$ glass. Comput Mater Sci 65:44–47. https://doi.org/10.1016/j.commatsci.2012.06.040
52. Finney JL (1970) Random packings and the structure of simple liquids. I. The geometry of random close packing. Proc R Soc A 319:479–493. https://doi.org/10.1098/rspa.1970.0189
53. Bernal JD, Finney JL (1967) Random packing of spheres in non-rigid containers. Nature 214:265–266. https://doi.org/10.1038/214265a0
54. Meraj Md, Pal S (2016) The effect of temperature on creep behaviour of porous (1at.%) nano crystalline nickel. Trans Indian Inst Met 69:277–282. https://doi.org/10.1007/s12666-015-0763-x
55. Lou H, Wang X, Cao Q, Zhang D, Zhang J, Hu T, Mao H, Jiang JZ (2013) Negative expansions of interatomic distances in metallic melts. PNAS 110:10068–10072. https://doi.org/10.1073/pnas.1307967110
56. Gangopadhyay AK, Blodgett ME, Johnson ML, Knight JM, Wessels V, Vogt AJ, Mauro NA, Bendert JC, Soklaski R, Yang L, Kelton KF (2014) Anomalous thermal contraction of the first coordination shell in metallic alloy liquids. J Chem Phys 140:044505. https://doi.org/10.1063/1.4861666
57. Kittel C (1996) Introduction to solid state physics, 2nd edn. John-Wiley and Sons, New York
58. Liu XJ, Xu Y, Hui X, Lu ZP, Li F, Chen GL, Lu J, Liu CT (2010) Metallic liquids and glasses: atomic order and global packing. Phys Rev Lett 105:155501. https://doi.org/10.1103/PhysRevLett.105.155501
59. Matsuura M, Sakurai M, Zhang W, Inoue A (2007) Local structures around Zr, Ni and Cu for the $Zr_{67}Cu_{33}$ and $Zr_{67}Ni_{33}$ metallic gasses. Mater Sci Forum 539–543:1959–1963. https://doi.org/10.4028/www.scientific.net/MSF.539-543.1959
60. Colín JG, Valladares AA, Valladares RM, Valladares A (2015) Short-range order in ab initio computer generated amorphous and liquid Cu–Zr alloys: a new approach. Physica B: Cond Matter 475:140–147. https://doi.org/10.1016/j.physb.2015.07.027
61. Foroughi A, Tavakoli R, Aashuri H (2016) Molecular dynamics study of structural formation in $Cu_{50}Zr_{50}$ bulk metallic glass. J Non-Cry Solids 432:334–341. https://doi.org/10.1016/j.jnoncrysol.2015.10.028
62. Mattern N, Jóvári P, Kaban I, Gruner S, Elsner A, Kokotin V, Franz H, Beuneu B, Eckert J (2009) Short-range order of Cu–Zr metallic glasses. J Alloys Compd 485:163–169. https://doi.org/10.1016/j.jallcom.2009.05.111
63. Wang Y, Yao J, Li Y (2018) Glass formation adjacent to the intermetallic compounds in Cu-Zr binary system. J Mater Sci Tech 34:605–612. https://doi.org/10.1016/j.jmst.2017.09.008
64. Sikan F (2017) Production and characterization of CuZr−RE based bulk amorphous/nanocrystal composite. Master's Thesis, Middle East Technical University
65. Baker H, Okamoto H (1992) ASM Handbook, Volume 03− Alloy Phase Diagrams. ASM International
66. Wu SY, Wei SH, Guo GQ, Wang JG, Yang L (2016) Structural mechanism of the enhanced glass-forming ability in multicomponent alloys with positive heat of mixing. Sci Rep 6:38098. https://doi.org/10.1038/srep38098
67. Luo WK, Sheng HW, Alamgir FM, Bai JM, He JH, Ma E (2004) Icosahedral short-range order in amorphous alloys. Phys Rev Lett 92:145502. https://doi.org/10.1103/PhysRevLett.92.145502
68. Sheng HW, Luo WK, Alamgir FM, Bai JM, Ma E (2006) Atomic packing and short-to-medium range order in metallic glasses. Nature 439:419–425. https://doi.org/10.1038/nature04421
69. Hwang J (2011) Nanometer Scale atomic structure of zirconium based bulk metallic glasses, Ph.D. Thesis. University of Wisconsin–Madison
70. Wang T, Zhang F, Yang L, Fang XW, Zhou SH, Kramer MJ, Wang CZ, Ho KM, Napolitano RE (2015) A computational study of diffusion in a glass-forming metallic liquid. Sci Rep 5:10956. https://doi.org/10.1038/srep10956
71. Sun Y, Zhang F, Ye Z, Fang X, Ding Z, Wang CZ, Mendelev MI, Ott RT, Kramer MJ, Ho KM (2014) Crystalline 'Genes' in Metallic Liquids. *ArXiv e-prints* 1714
72. Wei D, Yang J, Jiang MQ, Dai LH, Wang YJ, Dyre JC, Douglass I, Harrowell P (2019) Assessing the utility of structure in amorphous materials. J Chem Phys 150:114502. https://doi.org/10.1063/1.5064531
73. Hill MO (1973) Diversity and evenness: a unifying notation and its consequences. Ecology 54:427–432. https://doi.org/10.2307/1934352